TrueWind - Open Air Test Rig

Rolighed Thorsen, Gunhild; Wagner, Rozenn; Courtney, Michael; Pedersen, Anders Tegtmeier

Publication date:
2019

Document Version
Publisher's PDF, also known as Version of record

DTU Wind Energy E-Report-0184

TrueWind - Open Air Test Rig

Gunhild R. Thorsen, Rozenn Wagner, Michael Courtney and Anders T. Pedersen

DTU Wind Energy
Department of Wind Energy

DTU Wind Energy, Risø Campus,
Technical University of Denmark, Roskilde, Denmark

July 2019

Author: Gunhild R. Thorsen, Rozenn Wagner, Michael Courtney and Anders T. Pedersen
Title: TrueWind - Open Air Test Rig
Department: DTU Wind Energy

DTU Wind Energy E-Report 0184
July 17, 2019

ISSN:978-87-93549-52-4
ISBN:978-87-93549-52-4

Abstract (max. 2000 char)

In this project we compare the horizontal wind speed measured with a First class cup anemometer with wind speeds measured with three DTU short range Windscanners. Here a First class Thies cup is top-mounted on a 10 m meteorological mast equipped with various atmospheric sensors. The probe volume of the Windscanners are located at the same height as the cup, but 1.2 m southwest from the cup position. Prior to the cup measurements the wind speed measured with the Windscanners is compared with a sonic anemometer to check the validity of the setup.
In this report, the field experiment set up is described. The data quality was thoroughly checked. The sensitivity of the ratio between the cup anemometer and the WindScanner wind speed measurements to various conditions of speed, turbulence and temperature were investigated. The time series Windscanner data produced in this experiment will be used to validate the Accuwind model for cup anemometer classification.

Contract no:

Project no:
TrueWind

Sponsorship:
EUDP TrueWind project, journal number 64015-0635

Cover:

Pages: 48
Tables: 7
Figures: 34
References: 17

Technical University of Denmark
Frederiksborgvej 399
4000 Roskilde
Denmark
Tel. +4522506305
guth@dtu.dk
www.vindenergi.dk

Contents

1 Introduction

Cup anemometer is the primary sensor used by the wind industry to measure the wind speed for wind resource assessment and for accredited power performance measurement for certification and verification purposes. For those applications, measurements must be done with cup anemometer with a class better than 1.7A for flat terrain and 2.5B for and complex terrain[10]. The 1.7A class corresponds to a maximum wind speed error of 1% at 10 m/s and and the 2.5B class corresponds to a maximum error of 1.4% at 10 m/s. The sources of error in cup anemometry include the effects of the tower, the boom and other mounting arrangements, the anemometer design, the turbulent characteristics of the flow and the calibration procedure. Various types of cup anemometers have been shown to provide different wind speed measurements due to their angular response, dynamic effects and bearing friction characteristics [6]. Those characteristics have been extensively analyzed for five different types of cup anemometers in the ACCUWIND project [13]. Due to those effects, the cup response deviates from the reference calibration performed in a wind tunnel (according to IEC 61400-12-1 [10], Annex F) once the cup anemometer is placed in the open air, characterized by random wind fluctuations. IEC 61400-12-1[10] requires accounting for those deviations through an uncertainty term defined through the classification of the cup anemometer ([5]). The classification procedure takes place in three steps [14]: 1) the response of the cup anemometer to a defined range of operational parameters is evaluated through tests in a wind tunnel; 2) the characteristics of the cup anemometer are fitted to a realistic 3D cup anemometer model.; 3) the model is used to calculate the response under the range of operational conditions which are set up for the classification (IEC 61400-12-1[10], Annexes I and J). The ultimate verification of the model to predict the cup anemometer behavior would be to compare detailed field measurement with calculated anemometer response. This is one of the objectives of the TrueWind project.

This requires that the 3D wind field is accurately known in detail at the cup anemometer position. In practice the cup anemometer measurements are compared to simultaneous measurements from a co-located instrument. In most cases a sonic anemometer is used as reference ([5], [11]), since another cup would not enable us to distinguish the specific response of the tested cup anemometer. However sonic anemometers are not ideal references for this type of comparison since their measurements are disturbed by the flow distortion of their own supporting rods ([9]).

The DTU short range WindScanners (SRWS) system is offering a solution. The system is made of three continuous wave lidars with their beam focused and crossing in the same position thus providing a measurement of the 3D wind vector and the flow is not disturbed. For this specific study the WindScanner system was set up to measure at 10 m above the ground. The telescopes in the WindScanners are designed to have a probe volume of each of the scanner is 10 cm at this distance, which is comparable to a sonic anemometer (without the inconvenient of the flow distortion due to the rods). However, the prisms used for steering the beam induce astigmatism which is broadening the probe volume. The real probe volume is estimated in section 2.2.1

The purpose of this report is to provide a comprehensive description of the TrueWind Open Air Test Rig specifically designed for evaluating the cup anemometer response to wind field using the SRWS system as wind measurement reference, 1.2m away. Before their deployment, the line of sight (LOS) wind speed of each lidar was verified against a flywheel [12]. During the deployment, the WindScanner beams were carefully oriented to the same measurement position. The WindScanner measurement were compared to simultaneous measurements using a Metek sonic anemometer in order to validate the algorithm applied to calculate the three components of the wind vector (u,v,w) from the three LOS wind speeds. Finally the WindScanner was used as reference to estimate the response of the Thies First Class cup anemometer.

The SRWS time series data will be used as input to the Accuwind model[5] for direct comparison of the modeled cup response to the actual cup measurements. This will be described in a separate report.

2 Description of setup

The Open Air Test Rig was placed at the south end of the test site south of DTU Riso Campus. The OATR is surrounded by grass land and fields. The Roskilde fjord is on the North-West. The terrain follows a gentle slope of around 4% from the fjord on the west side of the OATR to the OATR and a gentle slope of about 3% from the OATR to the road on the east side of the OATR. A farm consisting of several houses and surrounded by trees is located on the south East at 160 m (max width, estimated from Google Earth, is around 140 m). In the 20 degrees direction is a row of 4 different wind turbines. A Digital surface map of the surroundings is shown in Figure 1.

The measurement campaign consists of two phases:

1. from the 03-04-2018 to the 17-05-2018, a Metek sonic anemometer was mounted on the top of the mast;
2. from the 22-05-2018 to the 31-07-2018, a Thies First Class cup anemometer was mounted on the top of the mast.

The WindScanner setup remained unchanged between the two phases.

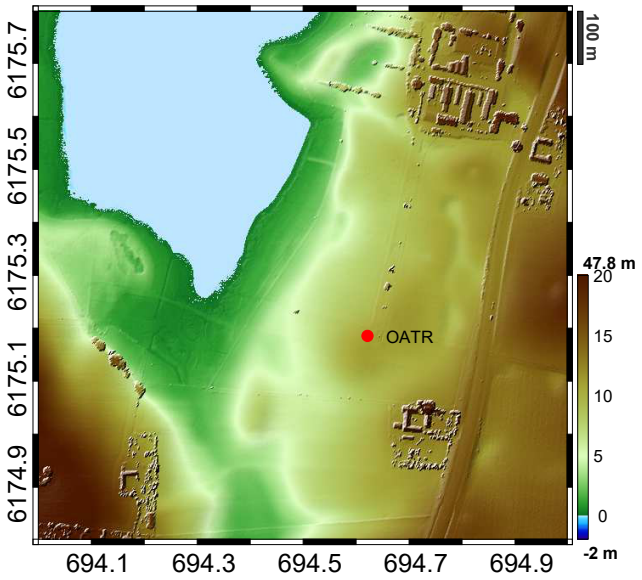

Figure 1. Digital surface map of the area around the position of the OATR (UTM32 WGS84). The red spot marks the position of the OATR. The color scale of the elevation has been truncated at 20 m.

2.1 OATR

The OATR consists of a 10m meteorological lattice mast. A vertical pole at the top of the mast enables us to install a sonic or a cup anemometer. The mast is furthermore equipped with either a cup or a sonic in 8 m, a wind vane and temperature sensor in 6 m and a humidity sensor and a pressure sensor in 2 m. These sensors enable us to track the different weather conditions during the measurement campaign. Three short range WindScanners (named R2D1, R2D2 and R2D3) are positioned around the mast so that their beams cross in a common measurement volume located 1.2 m south east of the top of the mast. The set up is shown in Figure 3 and Figure 4

and in figure 2 a detailed drawing of the mast instrumentation in the two measurement periods is shown.

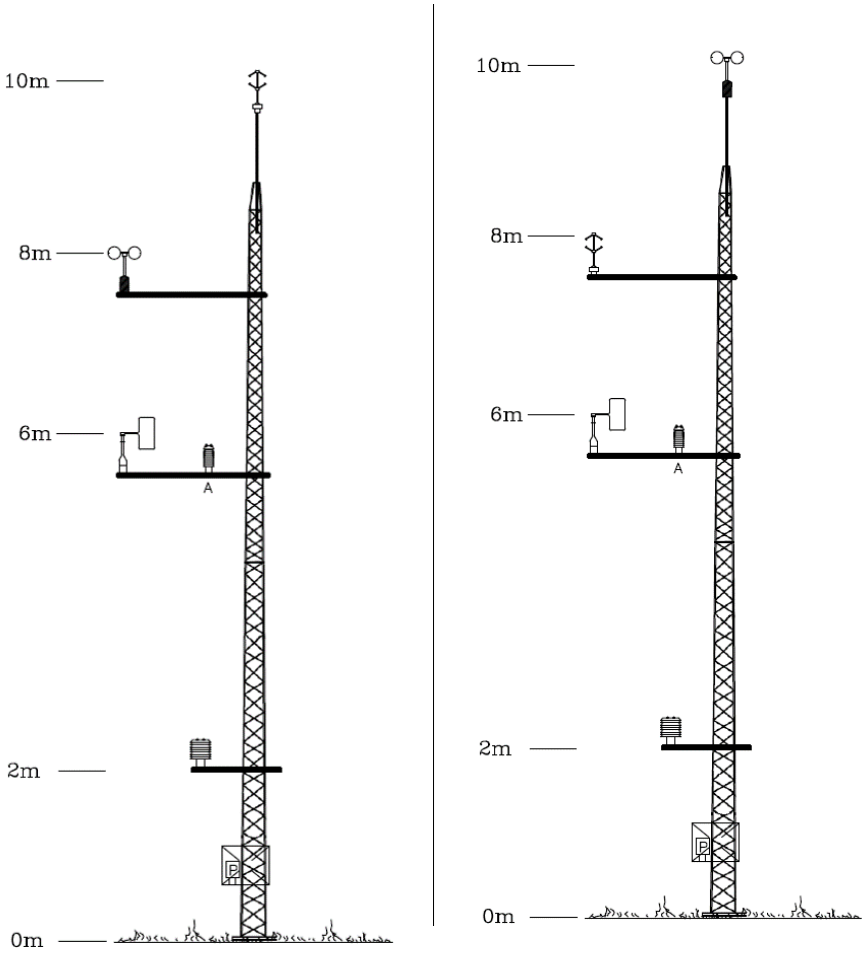

Figure 2. Instrumentation of the TrueWind mast during the measurement campaign. The campaign was divided into two periods. Left pane: Mast instrumentation of the period 1 (from 03-04-2018 to 17-05-2018). Right pane: Mast instrumentation of the period 2 (from 22-05-2018 to 31-07-2018). The Sonic in 8 m was only mounted in part of period 2(from 19-06-2018 to 31-07-2018)

2.2 Short Range WindScanner System

The DTU short-range WindScanner system consists of three continuous wave coherent Doppler lidars with DTU developed dynamically steerable scanner heads [17]. The scanner head consists of two prisms with a a 30° deflection angle. Before deployment, the line of sight (LOS) wind speed of each lidar was verified against a flywheel [12].

For this experiment the position of the focus and the laser beam is fixed throughout the period of the experiment.

2.2.1 Deployment and alignment procedure

In order to make sure that the three WindScanner were measuring at the same position, both the beam position and its focusing distance had to be checked for each lidar. An alignment ball made of low-density polyether was put in the position of the measurement volume of the scanners

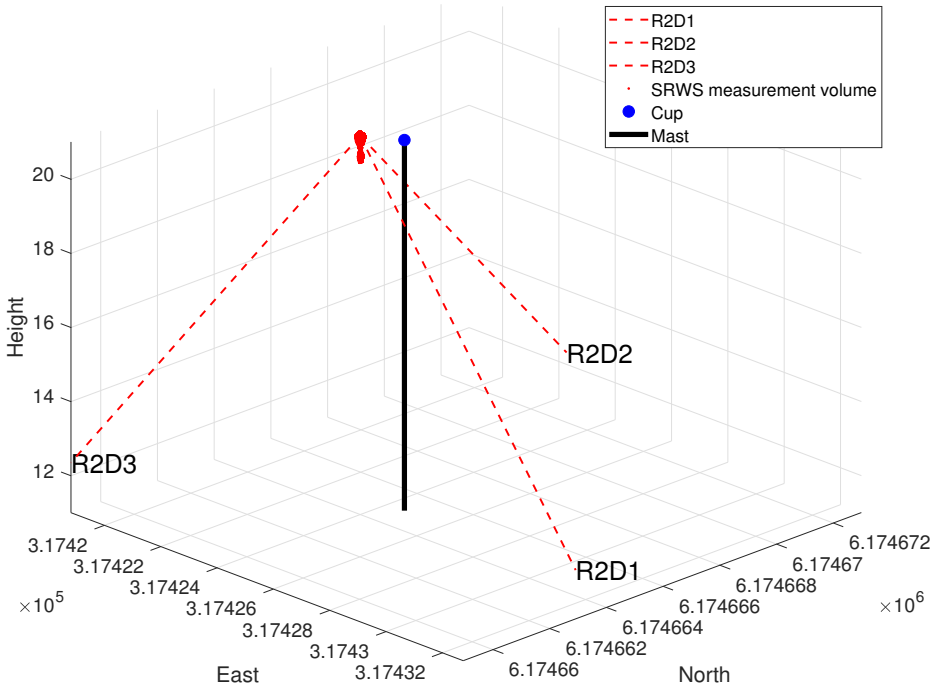

Figure 3. OATR setup seen from the side. The height is measured from sea-level an the dashed red lines indicate the beam path from each scanner head to the measurement volume

using a boom. The ball was mounted on a motorized vertical pole, which enabled the ball to spin. An example of the set up can be seen in figure 5 right pane. An infrared camera was used to locate the laser beams and the scanners where moved until the beam was visible at the center of the alignment ball. This was possible as the sky was cloudy, thus providing a dark background making the laser beam visible with the IR camera. Figure 5 left pane shows the R2D1 beam illuminating the alignment ball.

The position of the alignment ball, the center position of the outer prism of the SRWS systems and the position of the of the center of the alignment ball were determined using a Leica-Theodolite system[1]. The positions are listed in the Table 1. The uncertainties for the center position of SRWS are not the uncertainty given by the Leica-Theodolite system, but an uncertainty of where the beam is exiting the outer prism. Likewise the uncertainty of the measurement volume is the estimated uncertainty of the position of the crossing point of the beams. From these positions the azimuth and elevation angles for the direction of the laser beams and the direction between the cup/sonic and SRWS measurement volume were calculated. These are listed in Table 2. The azimuth, θ, is measured clockwise from the the north direction and the elevation, ϕ is measured from horizontal, positive pointing upwards. The direction of the beam is measured from the SRWS system measurement volume to the outer prism of the SRWS. As for the position of the beam, the angles are also have an uncertainty. These uncertainties are calculated in Appendix D.

The alignment was checked again 44 days after the start of the measurement to make sure that the WindScanners beam orientation had not changed. This time an alignment ball made of polystyrene was used (this material is more suitable than the polyether, which absorbs water and cannot be used in light rain) and a lift was used so the beam could be found using an NIR Detector Card close to the ball - this method does not require the use of an IR camera and can therefor be carried out on a sunny day (see Figure 5 middle pane).

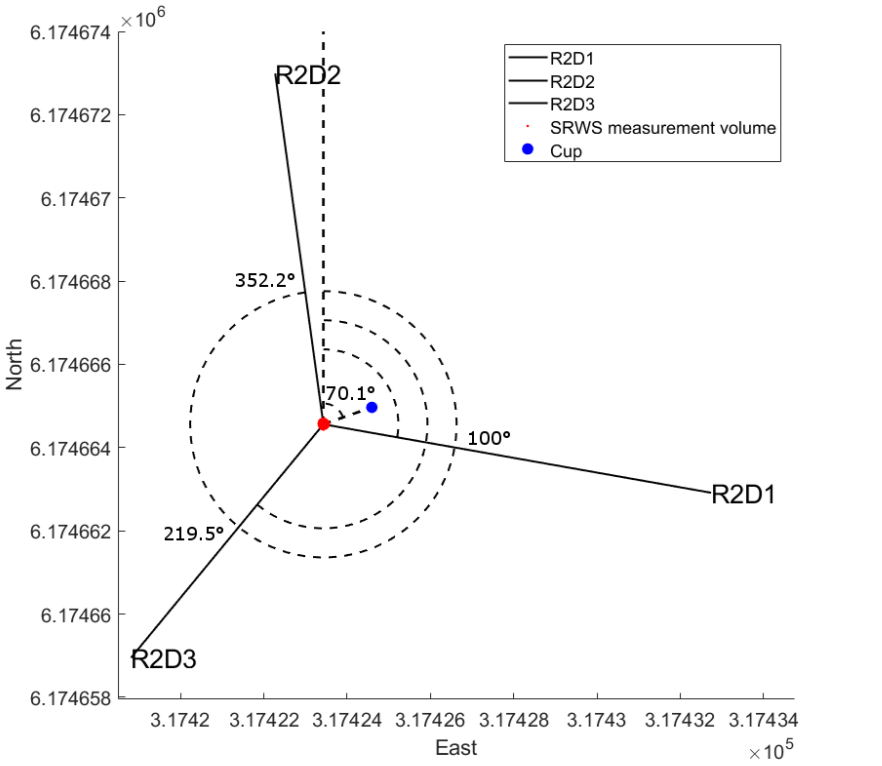

]

Figure 4. OATR setup seen from above.The solid black lines indicate the beam path from each scanner head to the measurement volume. The blue point indicates the position of the cup or sonic anemometer.

Figure 5. Left pane: R2D1 beam illuminating the alignment ball. The picture is acquired with an infrared camera. Middle pane: The alignment of the beams is checked. The position of the beams where checked using an NIR Detector Card. Right pane: Overview of the setup using the alignment ball. The alignment ball positioned on a boom south-west of the sonic anemometer.

The focus distance of the beam - for each WindScanner- was checked by moving the focus distance from positions in front of the the ball to positions behind the ball. This is practically achieved by moving the position of the optical fiber end relative to the focusing lens. When the light of the laser beam reflects of the rotating alignment ball a peak appears in the Doppler

Name	Eastern [m]	Northern [m]	Height [m]
Measurement volume	317423.43(5)	6174664.56(5)	20.90(5)
R2D1	317432.74(1)	6174662.92(1)	12.32(1)
R2D2	317422.27(1)	6174672.99(1)	12.32(1)
R2D3	317418.81(1)	6174658.95(1)	12.36(1)

Table 1. GPS-coordinates for the center of the outer prism of the three SRWS systems and for the measurement volume in UTM33 WGS84.

Name	θ [°]	ϕ [°]
Cup-SRWS	70.7	-
R2D1	100.0(3)	-42.2(2)
R2D2	352.2(3)	-45.2(2)
R2D3	219.5(4)	-49.6(2)

Table 2. Direction from the cup/sonic to the SRWS system measurement volume and Azimuth and elevation angles for each lidar beam. The azimuth, θ, is measured clockwise from the the north direction and the elevation, ϕ is measured from horizontal, pointing upwards, from the SRWS measurement volume position (origin of coordinate system).

spectrum of the measured signal corresponding to the speed of the ball. The amplitude of this peak depends on the power intensity of the beam when reflected on the ball. In figure 6 the maximum value of the power density spectrum (PDS) is plotted for each motor position. The focus position was scanned back and forth several times and the for each motor position an average of the maximum values is shown in Figure 6. The maximum value of the PDS will be highest when the focus is at the surface of the ball.

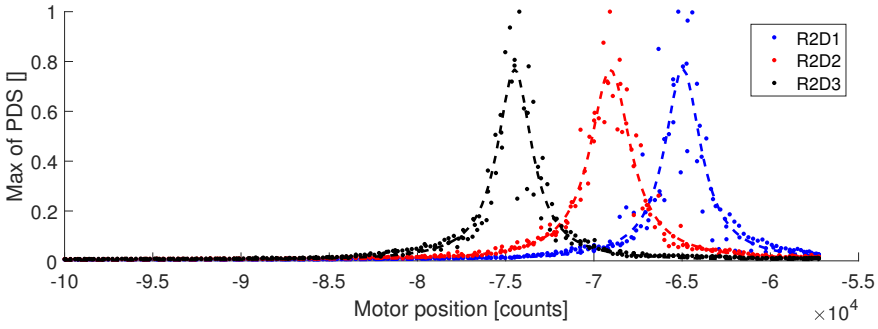

Figure 6. Normalized maximum power density for each motor positions. At each motor position the the PDS is an average of multiple measurements. The dashed lines represent the fits

The power intensity along the beam direction was assumed to be a Lorenzian distribution function:

$$\phi(x,s) = \frac{1}{\pi}\frac{z_R}{z_R^2 + (x-s)^2}. \tag{1}$$

where x is the distance from the focusing lens to the point where the intensity is measured, s is the distance between the transceiver and the focus point, and z_R is the Rayleigh range:

$$z_R = \frac{\lambda s^2}{\pi a_0^2}, \tag{2}$$

where λ is the wavelength of the laser beam and a_0 is the effective radius of the telescope. The distance from the transceiver to the ball, x, and the effective radius of the focusing lens

were calculated by applying a non linear fit to the PDS measurements using a scaled version of equation (1) and a_0, x, and a scaling factor as free parameters. The distance s is given from the motor position with the following formula:

$$s = f\left(1 + \frac{f}{-c_s m_0}\right). \tag{3}$$

Here f is the focal length, c_s is a conversion factor from motor position to distance. For this system $c_s = 0.1 \cdot 10^{-6}$m. By setting $s = x$ rearranging (3) to get m_0 and using the values in table 3 we find the position that focus motor should be set in order to focus in the surface of the ball. Finally the probe length was estimated using equation (2). The derived values from the fit shown in figure 6 are given in table 3.

	R2D1	R2D2	R2D3
a_0 [mm]	18.39	17.43	18.9
x [m]	12.79	12.05	11.2
Probe length($2 \cdot z_R$)[m]	0.48	0.47	0.35
λ [nm]	1565	1565	1565

Table 3. Effective radius of focusing lens, focus distance and probe length calculated from the fit shown in figure 6 and the specified laser wavelength of the SRWS.

2.2.2 Doppler spectra

The Doppler spectra are achieved through the emission of infrared (IR) laser radiation, with a 1.5 μm wavelength, in the atmosphere and subsequently by detecting the radiation back-scattered from aerosols. By detecting the beat signal between the transmitted light and the Doppler shifted light back-scattered from aerosols information about the Doppler shift is retrieved by performing a discrete Fourier transform of the signal.

The beat signal used to retrieve the Doppler spectrum is sampled at a frequency of 120 MHz which permits a maximum $\pm$60 MHz to be detected enabling the instrument to detect a maximum wind speed of $\pm$47 m/s. With a 512 point discrete Fourier transform (DFT) the difference between two frequency bins is 234 kHz corresponding to a difference in wind speed of 18 cm/s. In a normal Fourier spectrum, the spectrum is mirrored making a signal with the Doppler frequency $\Delta\omega$ and $-\Delta\omega$ indistinguishable. Using in-phase and quadrature detection [3], the instrument is able to distinguish between the sign of the Doppler frequency.

2.2.3 LOS speed estimator

Since the WindScanner retrieves wind signal along the probe volume, the Doppler spectrum will correspond to a distribution of wind speeds. The raw spectra are flatten and a threshold is applied to remove noise before the mean wind speed is estimated using a median estimator[4]. From calibration experiments, the uncertainty on the LOS wind speed estimation the uncertainty of the LOS wind speed is estimated to be 0.2%[12].

2.3 Data acquisition system

Data from the mast instruments, except the sonic, was collected in a Data Acquisition Unit called DAU, which sample the electrical signals from the mast instruments at a sampling rate of 35 Hz, converts them to binary numbers and transfers the data via serial connection. The data from the sonic is sampled at a rate of 20 Hz, locally processed and transferred via a serial connection with a data rate of 20 Hz. The three WindScanners each produce a Doppler spectrum at a data rate of 20 Hz, which is locally processed to get the estimated radial wind speed from each WindScanner (see section 2.2.3). The wind speed together with information about data quality and more are

transferred via a serial connection with a data rate of 20 Hz. All data are then collected with a dedicated data acquisition program called DaQWin, which has been developed in LabView. The program receives telegrams via a serial connection with data from the different instruments, stores the measurements with a time-stamp at a predefined sampling rate and in the case with the data from the DAU, the program re-scales the data to physical units using calibrations from the different mast instruments. In this case a sampling rate of 20 Hz was chosen. The advantage of using the same computer to collect and set time stamps for the measurements is that it eliminates the risk of drift in time between the different data acquisition systems.

Data from the mast mounted instruments and the estimated wind speed from the WindScanner system were collected in DaQWin from the beginning to the end of the campaign. A program able of collecting the Doppler spectra from the SRWS was developed during the campaign and thus the Doppler spectra were only saved from the 25-06-2018 to 31-07-2018.

2.4 WindScanner data filtering

To ensure the quality of the WindScanner data, several filters were applied on LOS wind speed of each of the WindScannes:

- removing Q = NaN values
- de-spiking of LOS wind speed time series using the method from Goring & Nikora [8].
- Removing repeated data from LOS speed time series

The Q-value is defined as the ratio between the sum of the spectrum in the frequency bandwidth +/- 1 bin around the estimated velocity bin and the total power of the spectrum. A Q-value is provided for each estimated LOS wind speed (20Hz data). During the data analysis, it was noticed that when the Q-value was NaN the LOS speed was always 0 m/s. The NaN Q-value indicates that there has been not non-zero values in the spectrum. This can happen if the wind signal amplitude of the signal is lower than the threshold and thereby there is no power in the signal.

In Figure 7, an example of a time series of the LOS speed measured with R2D3 is shown. In the raw data (black line) it is clearly seen that there is a lot of wind speed equal to 0 m/s. This would pull the 10-min average artificially down. By removing wind speeds with a corresponding Q = NaN all of these artificial measurement points are removed.

When the Q = NaN data were removed, many spikes were remaining in the time series (see blue line in Figure 7). These spikes were removed using the de-spiking method described in [8]. The result of removing Q = NaN and the de-spiking can be seen as the red line in figure 7.

In some periods during the measurement campaign the WindScanner system was not working and therefore no data was sent to the DaQWin program. In that case the DaQWin program would repeat the last received data point and set a flag for each scanners indicating that the sample has been repeated. By filtering on these flags, repeating data is removed. When the data has been filtered the reconstruction described in the following section is applied. All filtered and reconstructed data are saved in a database. To assess the data availability of the 10-min statistics a flag is set if data from at least one of the scanner were set to NaN. When the LOS speed 10-min statistics were calculated, the data availability was also calculated as the ratio between the number of available data after filtering and the number of data before filtering in the 10 min period . For the data set shown in Figure 7, the data availability after applying the three filters is 36%.

2.5 Reconstruction of u, v and w

In order to compare with the sonic the LOS wind speeds from the three different wind scanners are converted into a 3D wind vector. The 3D wind vector is here defined by the three components $V_{wind} = (u, v, w)$. Here u is component of the wind pointing towards east, v is the component of the wind pointing toward north and w is component of the wind pointing upwards. The LOS wind speed measured with each of the WindScanners can be expressed from the 3D wind vector by

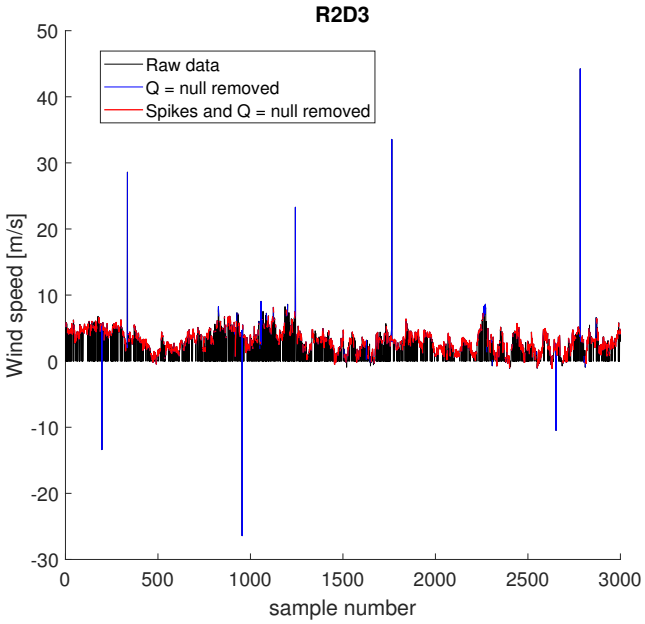

Figure 7. 20 Hz LOS measured with R2D3 from the 10- min period 04-10-2018 22:50 to 23:00. On the first quarter of the data is plotted. In this 10-min period 64% of the data is removed.

finding the dot product between V_{wind} and the direction of the laser beam:

$$V_{wind} \cdot \vec{n} = V_r = \sin(\theta)\cos(\phi)u + \cos(\theta)\cos(\phi)v + \sin(\phi)w. \tag{4}$$

where $\vec{n}$ is the unit vector pointing in the direction of the laser beam, θ and ϕ are respectively the azimuth and elevation angles of the laser beam direction (given in Table 2. For the setup used in this campaign the LOS wind speed is positive when the wind direction is towards the WindScanner. In this convention, the azimuth is measured from north positive clock-wise and the elevation angle from horizontal, positive upwards. By having three SRWS systems a set of three equations in the form of equation (4) can be written. By solving these equation for u, v and w the 3D wind vector is derived. A derivation of the u, v and w component of the wind vector can be found in appendix D.

From the reconstructed u, v and w the wind direction

$$\Theta = \arctan\left(\frac{-u}{-v}\right), \tag{5}$$

the horizontal wind speed

$$V_{hor} = \sqrt{u^2 + v^2}, \tag{6}$$

and the inflow angle

$$\Phi = \arctan\left(\frac{w}{V_{hor}}\right), \tag{7}$$

can be calculated. Since there is an uncertainty on the on the angles and the estimated LOS wind speed there will also be an uncertainty on u, v, w and V_{hor}. This uncertainty is calculated in Appendix D. The uncertainty on the V_{hor} is calculated to be up to 0.5%. It is important to note that the uncertainty contribution from the angle uncertainty is not expected to be a random uncertainty. Therefor it is expected that this uncertainty will result in a bias rather than scatter in the measurements.

3 Plausibility check with sonic anemometer

In the first phase of the measurement campaign a Metek USA-1 basic 3D ultrasonic anemometer [2] was installed on the top of mast. The sonic provides wind speed in 3 orthogonal directions, X(horizontal), Y(horizontal) and Z(vertical). The purpose was to validate the algorithm applied to calculate u,v,w from the LOS speeds from the three SRWS. Data were acquired with this set up for 44 days (from the 03-04-2018 to the 17-05-2018). For this test the 20Hz data was averaged and 10-min values have been compared.

3.1 Data correction and filtering

In order to be able to compare the SRWS data with the sonic data some corrections had to be made. The corrections are listed below:

- Sonic 2d correction removed
- Sonic 3D correction applied
- Direction of sonic aligned with north (turned 11 °)
- data from the period 04-13-2018 00:00 to 04-18-2018 00:00 removed

The sonic anemometer measures the wind from the three sets of probes attached on a metal-frame. To correct for 3D flow distortion originating from the metal-frame [15] first a default 2D correction is removed and the then a 3D correction is applied.

When the sonic was installed on the top of the mast, it was not aligned with north meaning that X and Y would not correspond to u and v. A Leica-scan of the sonic(see Figure 8 left pane and Figure 8) right pane was used to determine the misalignment with north, by fitting a plane to the three sides of the box just below the sonic. The results from the fit are given in Table 4. To correct for this misalignment the X and Y components of the wind speed from the sonic were rotated by 11 ° around the Z-direction.

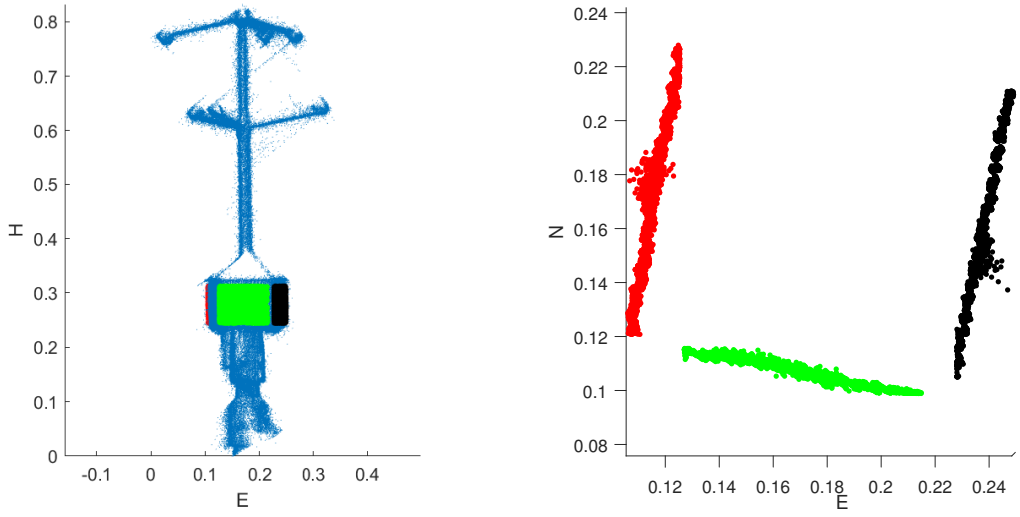

Figure 8. Left pane: Leica scan of sonic. The red, black and green points are selected to find the misalignment with north. Right pane: Fitted sides of the sonic box, seen from above.

In the period 04-13-2018 00:00 to 04-18-2018 00:00, the sonic was not sending data to DaQwin and the same value was repeated. These data points were removed.

Side #	Angle [°]
1	11.44
2	11.21
3	10.35
Average	11.0(6)

Table 4. Results from fitting a plane to the points shown in figure 8 right pane and calculating the angle that the sonic should be rotated in order to align it with north.

The correction of the SRWS data is explained in section 2.4. Furthermore the following conditions were applied to the data:

- data availability of the lidars >90%.
- Horizontal wind speed of sonic > 2 m/s

3.2 LOS speed comparison

The line-of-sight speed measurement of each WindScanner was compared to the sonic wind speed measurements (X,Y,Z) projected onto the LOS direction, using equation (4) with the angles from Table 2, (see Figure 9). The measurements show relatively good agreement on average. However R2D1 WindScanner shows a systematic underestimation of about 4.5% to the sonic wind speed. TheR2D3 WindScanner agrees well on average, but the scatter is significantly larger than for the two other WindScanners (R^2 below 0.9990).

In figure 10 the difference in V_{LOS} between the WindScanner and the sonic anemometer is plotted as a function of wind direction. For all WindScanners, the scatter i larger for wind directions around 140°. This may be due to a the wake of the farm (ensmeble of building and trees) located at about 160 m away from the OATR in this direction. However, the largest deviation (with large scatter) is observed for R2D1 for wind directions between 230° and 300°.

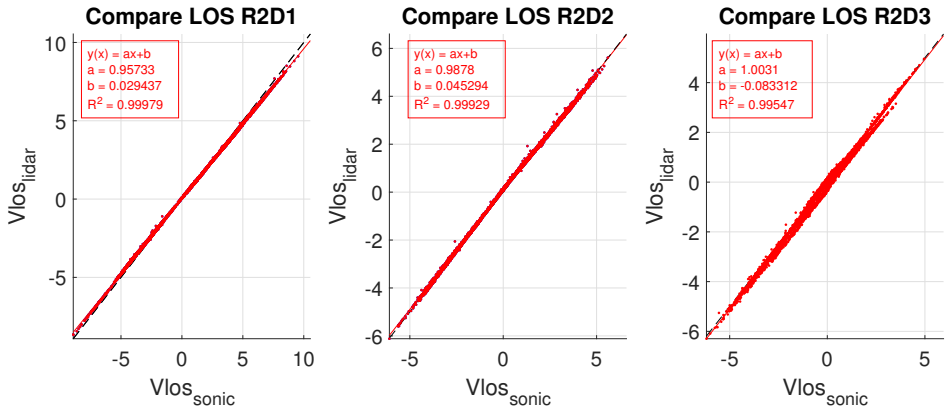

Figure 9. Comparison between VLOS of the each of the SRWS and the projected VLOS from the sonic data

3.3 Comparison of reconstructed V_{hor} and inflow angle

In this section the wind vector reconstructed from the the SRWS system measurements is compared with the sonic wind vector. In Figure 11 the horizontal wind speed measured with SRWS and the Sonic are compared. The WindScanners wind speed is lower than the sonic wind speed. This is consistent with the lower LOS speeds from all the WindScanners observed in Figure 9. There is more scatter for wind speeds below 8 m/s than for wind speed above 8 m/s.

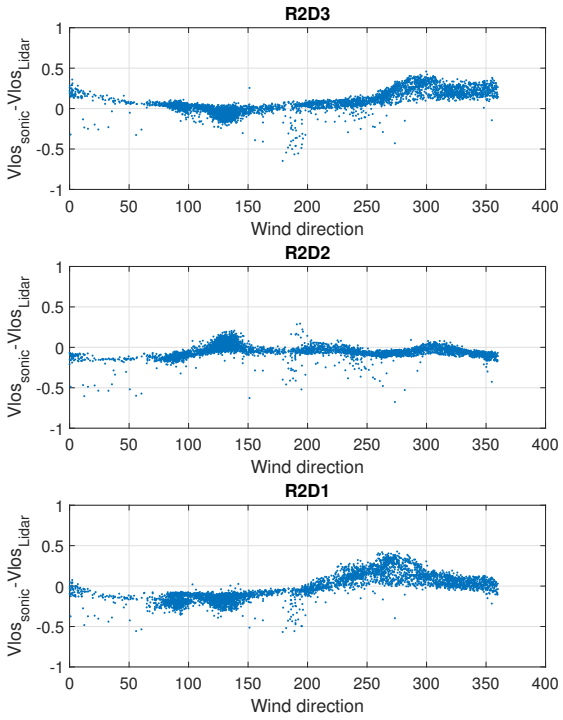

Figure 10. Difference in wind VLOS between sonic and lidar as function of wind direction.

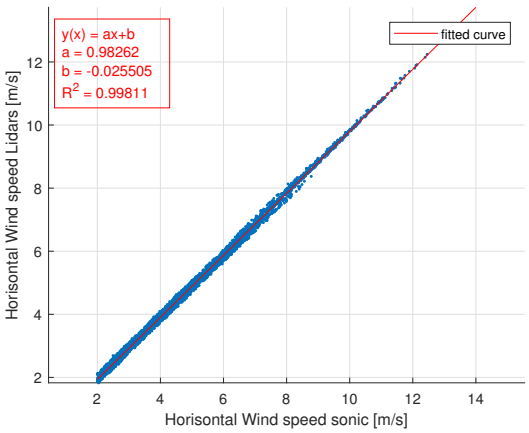

Figure 11. Comparison between horizontal wind speed measured with the SRWS and the sonic horizontal wind speed

The inflow angle measured with the SRWS is compared to the sonic inflow angle in Figure 13. Clear deviations appear between the measurements from the two instruments. The sonic measurements indicate that the inflow angle varies mainly between -2° and 2°, whereas the SRWS measurements go from -4° to +3°. Surprisingly, two groups distinct groups of data point appear. Further investigation has shown that the two groups were related to wind direction below and above 190°. In Figure 12 the difference between the inflow angle measured by the two instruments was plotted as a function of wind direction. It looks like the SRWS is measuring higher inflow angle for wind direction above 190° and a lower inflow angle for wind direction below

190°. This is also seen in the figure 13 where the inflow angle measured with the lidars is plotted against the inflow angle measured with the sonic. Here it looks like the data comes in two do-

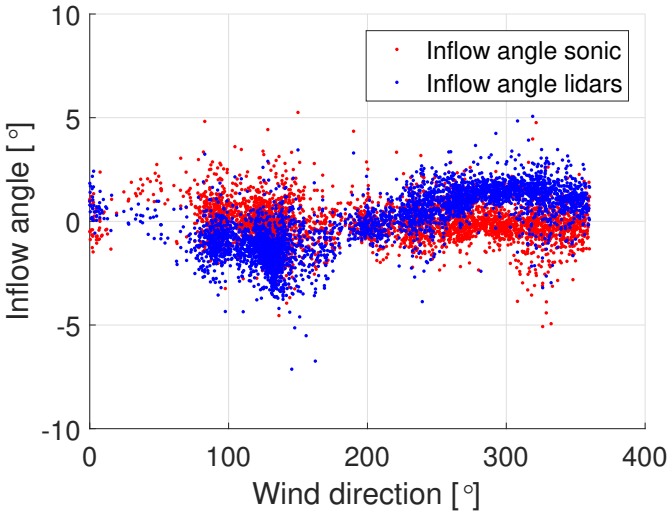

Figure 12. Comparison between inflow angle measured with the sonic and SRWS respectively

mains; one where wind directions are above 190° and one where wind directions are below 190°. The sonic and the lidars are clearly measuring different inflow angle depending on the wind direction. It is hard to determine whether it is the sonic or the lidars that are measuring wrong, but these plots suggest tat care should be taken when looking at the inflow angle.

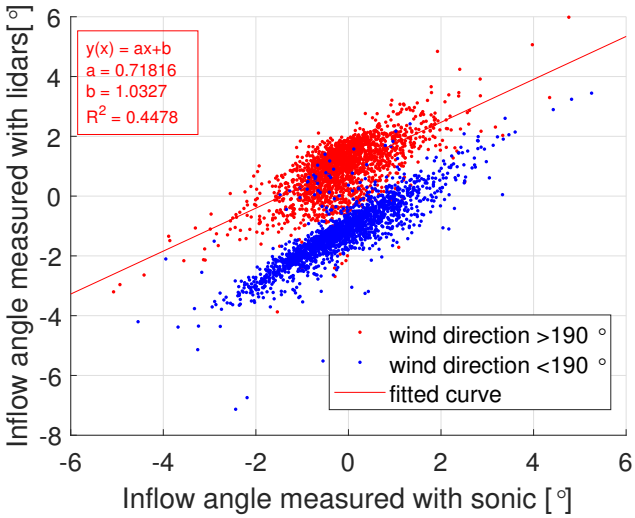

Figure 13. Comparison between inflow angle measured with the sonic and inflow angle measured with the lidars.

No explanation has been found for these differences. The beam angles of the SRWS have been checked twice with consistent results. Furthermore, given the terrain slope of 2-3° from the west to the east of the OATR, the variations shown by the SRWS measurements could be plausible: negative (downward) inflow angles from the East and positive (upwards) inflow angles from the west. If the sonic was tilted downwards by 2° towards the west, it could result in underestimated flow angles. However such a small tilt of the sonic would be difficult to check.

4 Comparison between a Thies cup and the SRWS system

In this section the comparison between the 10-min statistics of the horizontal wind speed measured with the Thies cup and the SRWS system is presented.

4.1 Data filtering

No filtering or correction has been applied to the time series of the Thies cup data. The SRWS 10 min statistics were prepared as described in 2.4. The 10 min data were filtered as follow:

- Thies cup wind speed $>$ 2m/s - a cup anemometer requires a minimum wind speed to start rotating and the data acquisition system has a lower limit of the rotational frequency that can be measured.
- 200° $<$ wind direction $>$ 360° - so wind sectors for which the OATR is in the wake of the turbines and the SRWS measurement volume is in the wake of the cup anemometer are discarded.
- SRWS data availability $>$ 90% - explained below;
- min(|R2D1 LOS speed|)>0.01 m/s - explained below.

Due to the filtering of the WindScanner data, some data are removed in the 20 Hz data. In figure 14 the ratio between Thies wind speed and SRWS wind speed as a function of data availability in the 10-min period is plotted. It is clear that for low data availability the ratio deviates more than for high data availability. Therefore, a 90% threshold was chosen to ensure good data quality. However, When the low availability data has been removed we still see some data points that

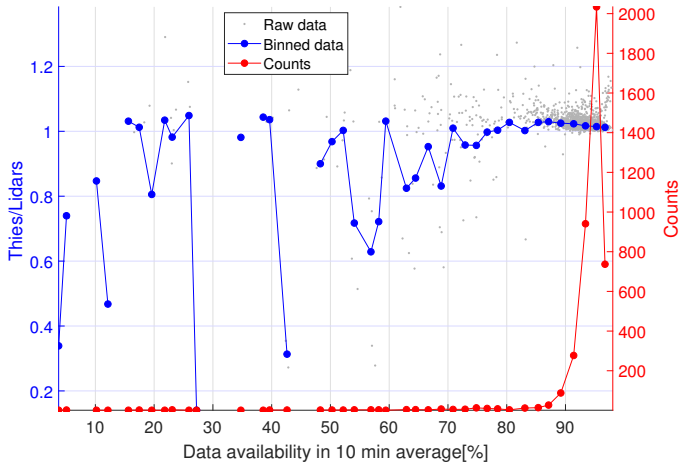

Figure 14. Ratio between Thies cup anemometer and SRWS horizontal wind speed as a function of SRWS data availability in the 10-min period. For bin-averaged data, the bin-size is 2%.

deviates significantly from the rest of the data. In Figure 15 the ratio between the Thies cup and the SRWS wind speeds is plotted as a function of time. There are some periods where the data deviates significantly more from the the rest of the time period. One of the outliers was investigated more closely by looking at the 20 Hz data of the WindScanners. In Figure 16 the LOS wind speed measured with each WindScanner is plotted for the period period 13-07-2018 23:40 to 23:50. For some samples, the R2D1 WindScanner provided very low wind speed compared to the rest of the data. An investigation of other outliers showed that R2D1 also here sometimes

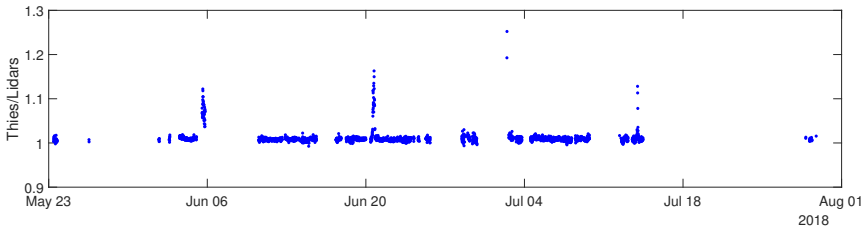

Figure 15. Ratio between Thies cup anemometer and lidar horizontal wind speed as a function of SRWS time.H ere low availability data has been removed.

measures a too low wind speed compared to the rest of the data. The fact that this only happens for one of the WindScanners, suggests that it is failure of the instrument and not caused by the ambient conditions, since this would affect all three WindScanners. For the period 07-13-2018

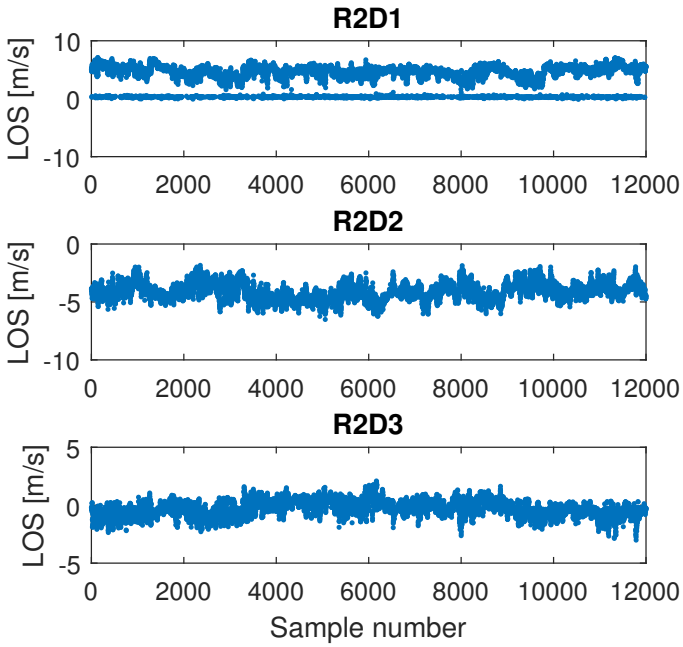

Figure 16. LOS wind speed measured with the three systems plotted for the period 13-07-2018 23:40 to 23:50.

23:40 to 23:50 the spectra has been saved and therefor those are investigated too see what caused the problem. In Figure 17 an example of a spectrum from the WindScanners R2D1 and R2D2 respectively is shown. For both systems we see a clear peak in the spectrum at ± 5 m/s for the R2D1 and R2D2 respectively, corresponding to the wind signal. However, for the R2D1 we also see a signal at almost zero wind speed. These spectra show that the low LOS wind speeds are caused by DC-noise in the spectrum. The origin of this noise has not been found, but it should be investigated for future experiments.

In order to remove periods where there has been DC noise i R2D1, we looked at the minimum value of the absolute R2D1 LOS wind speed in each 10-min period. In Figure 18 the ratio between Thies cup and SRWS system wind speeds is plotted as a function of the 10-min minimum absolut value of R2D1 LOS wind speed. All the data points with a wind speed ratio larger than 1.3 have a minimum absolute R2D1 LOS wind speed below 0.01m/s. All data with a minimum absolute R2D1 LOS wind speed below 0.01m/s were removed. This filter removed all the outliers, but it has also removed data that were not outliers (good agreement between Thies cup and SRWS data).

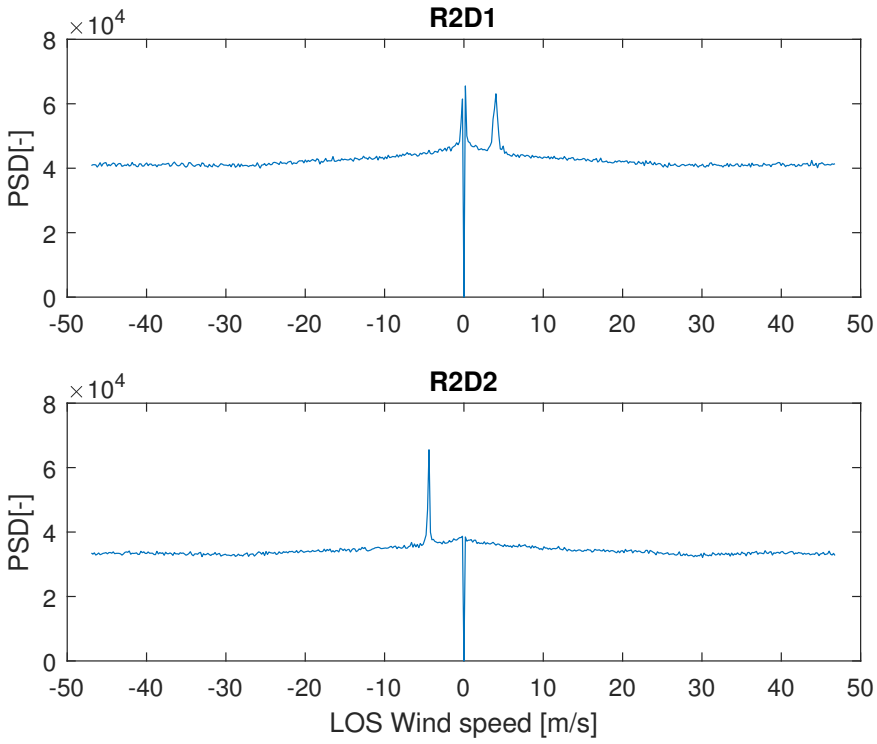

Figure 17. Single Doppler spectrum from period 07-13-2018 23:40 to 23:50 shown for R2D1 and R2D2

This would mainly periods where the wind direction was almost perpendicular to the R2D1 laser beam or a very low wind speed. Wind direction perpendicular to R2D1 beam direction would be within two small sectors around wind directions 190 ° and 10 ° respectively. Since those sectors were already removed these sector due to effects of obstacles(farm and terrain), this would not affect the data analysis.

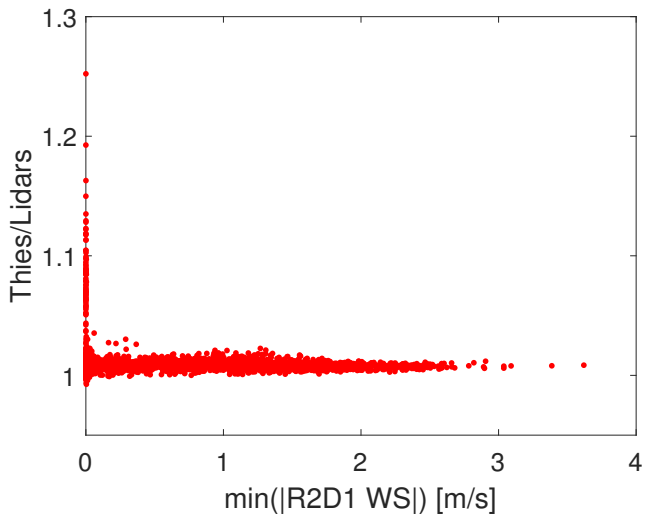

Figure 18. Ratio between Thies cup and SRWS system horizontal wind speeds as a function of 10 min minimum value of absolute R2D1 LOS wind speed

4.2 Mean wind speed and cup anemometer calibration

In Figure 19, the horizontal wind speed measured with Thies cup anemometer is plotted against the horizontal wind speed measured with the WindScanners. Two different linear regressions were applied to the data; with and without offset:

$$V_{Thies} = a1 \cdot V_{SRWS} + b1, \tag{8}$$

$$V_{Thies} = a2 \cdot V_{SRWS}. \tag{9}$$

Here $a1$, $b1$, and $a2$ are the fitting parameters and V_{Thies} and V_{SRWS} are the horizontal wind speed measured with the Thies cup and the WindScanner system respectively.

The Thies cup anemometer was calibrated at Deustche WindGuard GmbH (DWG) prior to the measurement campaign (20/2-2018). The results from the linear regressions are given in Table 4.2.

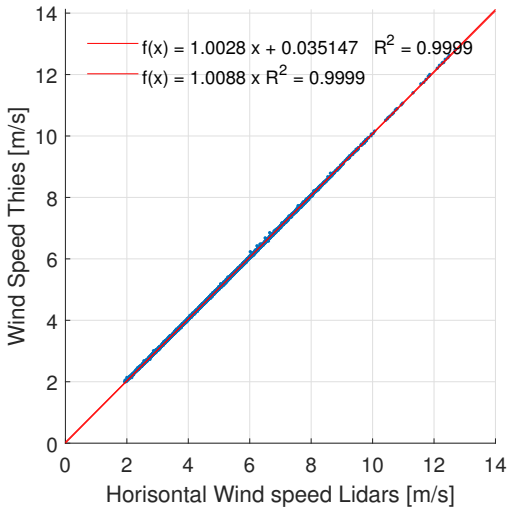

Figure 19. Scatter plot of the 10 min mean horizontal wind speeds given by the Thies cup (using the first calibrations from DWG) and the SRWS.

Calibration			Correlation fit			
	Gain	Off-set	a1	b1	a2	R^2
DWG[a]	0.04599	0.2395	1.0028	0.035	1.0088	0.9999

Table 5. Thies cup calibration constants from wind tunnel and regression coefficients for linear regression with and without offset between cup and SRWS data

[a] Calibration done at Deutsche WindGuard Wind Tunnel Services GmbH on the 20/2-2018. Certificate no. 1810801

4.3 Turbulence intensity

The main purpose of the SRWS is to measure the reference 10 min mean horizontal speed in order to observe deviations from the cup anemometer due to environmental conditions, especially turbulence intensity. Since lidars are usually not providing the same TI as cup anemometers due to the volume measurement and the cross contamination effect (ref from A. Sathe and J.Mann), it is relevant here to also compare the TI measurements from the SRWS system and the cup anemometer.

In figure 20 the TI measured with the cup is plotted against the TI measured with the WindScanners. A linear fit is applied to the data and it shows that the WindScanners are in general measuring a higher TI than the cup. Lidar measurements over a volume results in filtering out the small scale turbulence and in underestimating the TI. However, in this configuration, the focus distance of the three WindScanners is relatively short and thus the probe volume is small (see Table 3). Overestimation of TI by the SRWS may be explained by the cross contamination of the horizontal speed variance by the fluctuations of the vertical component of the wind (because the WindScanners beam is not horizontal) or/and by noise in the measurements from one or several of the WindScanners ([16]). Possible noise in the measurement is supported by the 2 parametric regressions that results in a gain of 0.9901 and an offset of -0.641. Cross contamination from the vertical component of the wind is expected to result is more random error.

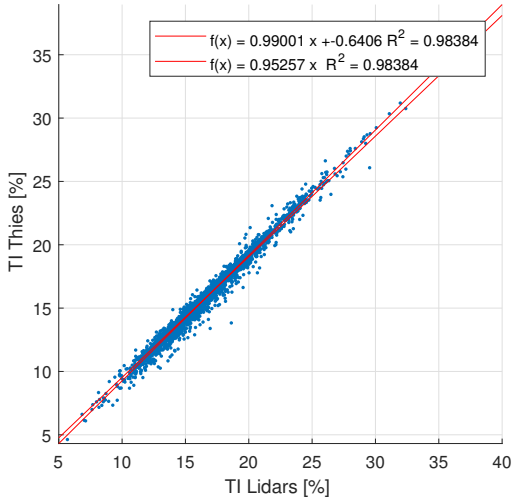

Figure 20. Scatter plot of the turbulence intensity measured with SRWS system and Thies cup anemometer.

5 Sensitivity of cup anemometer

In this section the ratio between the horizontal wind speeds measured with Thies cup and the SRWS system are shown as a function of various free air ambient parameters: wind direction, wind speed, temperature, turbulence intensity and inflow angle. The objective was to observe any sensitivity of the Thies cup anemometer to those parameters. The SRWS system was used as reference and assumed to provide the "true" wind speed (as lidar measurements are not expected to be sensitive to those parameters).

The following sensitivity analysis was performed on the same data set as the one described and used in section 4 (see description of filtering in 4.1). Furthermore wind speeds below 4 m/s were discarded for all figures in this section except for Figure 21 (see explanation in section 5.1). The Thies cup wind speeds were obtained using the calibration done before the measurement campaign at DWG.

5.1 Sensitivity to the wind speed

- Most of the data have a wind speed between 2 to 10m/s.
- The wind speed ratio increases for wind speeds below 4m/s. The cup calibration is only

valid for wind speed above 4m/s. Therefore wind speeds below 4 m/s were filtered out for the sensitivity analysis . Nevertheless the wind speed ratio is still larger for wind speed range 4 to 6m/s than for the rest of the data set.

- The wind speed ratio decreases as the wind speed increases up to 8m/s. However there are very few data available for wind speeds above 9m/s.

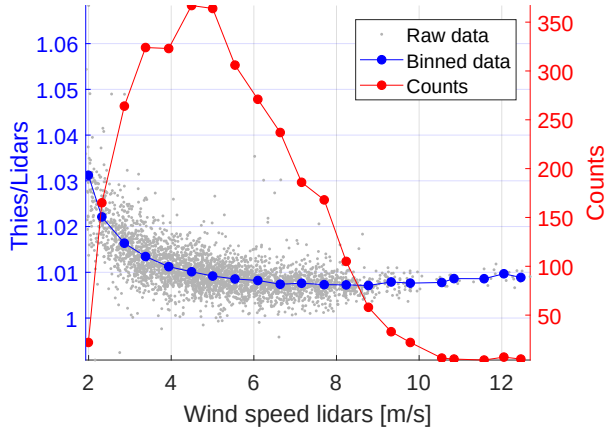

Figure 21. Ratio between horizontal wind speed measured with the Thies cup and the SRWS system as a function of SRWS horizontal wind speed

5.2 Sensitivity to wind direction

- The prevailing wind directions (for the wind speed above 4m/s) are between 260 ° and 320 °, as shown in Figure 22.
- Within this wind sector, the mean wind speed ratio decreases slightly and the scatter tends to increase (23). This may be related to the lower wind speeds towards the WNW direction.
- Those scatter are most likely due to variations of the cup anemometer response. In Appendix D, a model of the SRWS wind speed measurement uncertainty has shown that there is a bias which varies with the wind direction. The mean value of the SRWS wind speed within a direction bin is expected to have a very small uncertainty.

5.3 Sensitivity to Turbulence Intensity

- Since we had doubts about the TI measured by the SRWS system, the cup TI has been used as reference for this sensitivity plot, see Figure 24.
- Most of the cup TI ranges from 11% to 20%.
- There is no clear variation of the mean ratio in Figure 24 and the scatter is rather large. Nevertheless, the mean ratio is slightly increasing when the data are binned according to wind speed (Figure 25). According to previous observations, the ratio is larger for lower wind speeds. Yet, these remain small variations in comparison to the scatter.

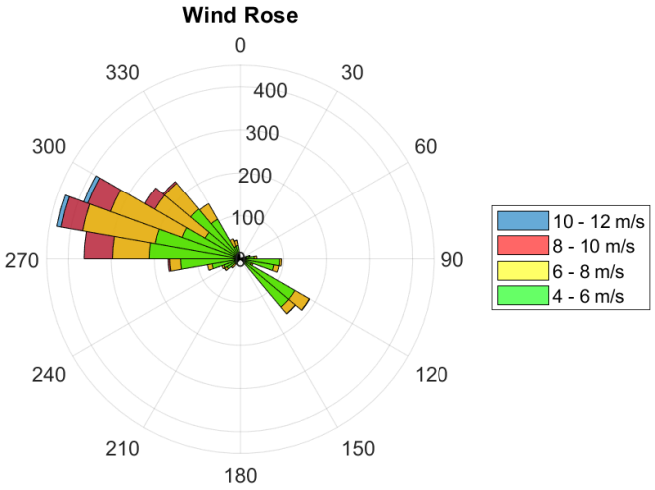

Figure 22. Wind rose showing the 10-min mean wind speed distribution per 10 ° wind direction sector. In this plot the wind direction filter has not been applied.

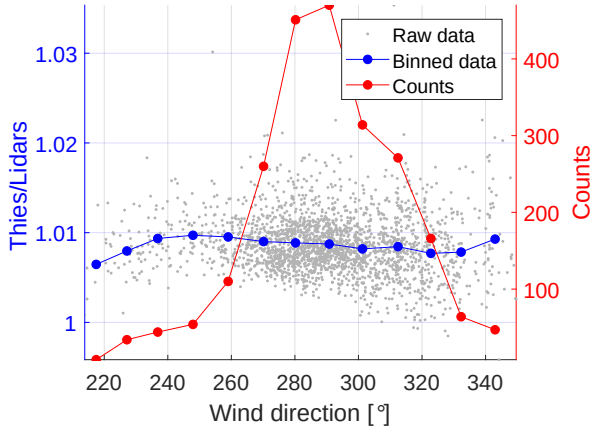

Figure 23. Ratio between horizontal wind speed measured with the Thies cup and the SRWS system as a function of SRWS wind direction

5.4 Sensitivity to temperature

- The air temperature was mostly between 14 °C and 20 °C for most data.
- The wind speed ratio slightly increases with temperature. In Figure 29, the wind speed ratio increases with temperature for high TI (above 15%).

5.5 Sensitivity to inflow angle

- The range of inflow angle is very limited since the OATR is placed in relatively flat terrain. The slight terrain slope from west to east may explain that the mean inflow angle is around 1.7°.
- Given the very narrow range of inflow angle it is not possible to observe any sensitivity of the wind speed ratio to the inflow angle.

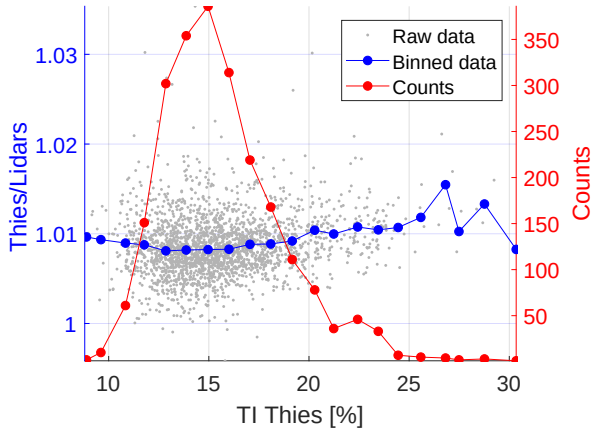

Figure 24. Ratio between horizontal wind speed measured with the Thies cup and the SRWS system as a function of Thies cup turbulence intensity

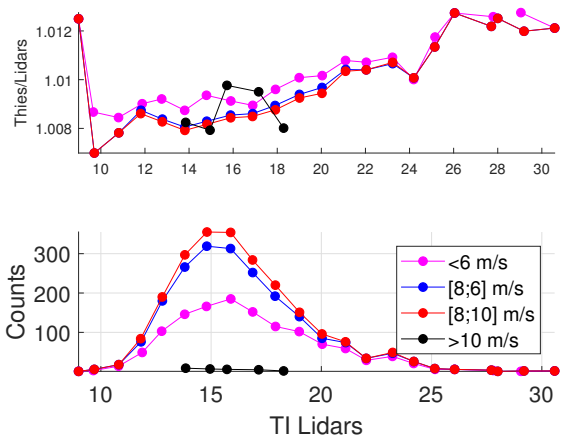

Figure 25. Ratio between horizontal wind speed measured with the Thies cup and the SRWS system as a function of SRWS turbulence intensity for different wind speed intervals.

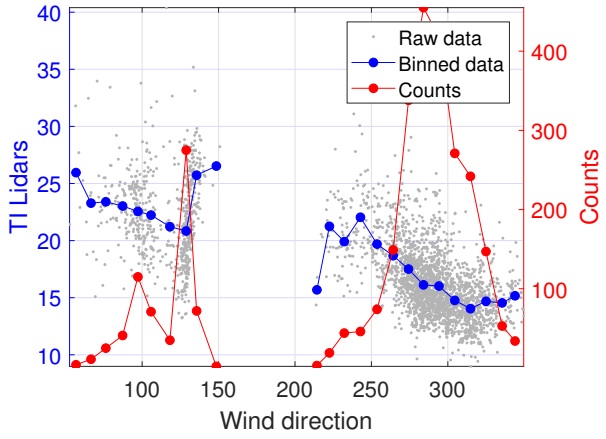

Figure 26. SRWS system TI as a function of SRWS system wind direction. In this plot the wind direction filter has not been applied. The reason why there are no measurements at wind directions from 150 ° to 190 ° is that we filter on low absolute LOS wind speeds for R2D1.

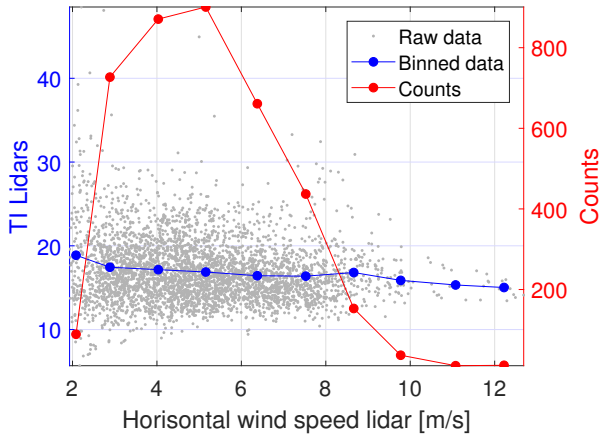

Figure 27. SRWS system TI as a function of SRWS system horizontal wind speed

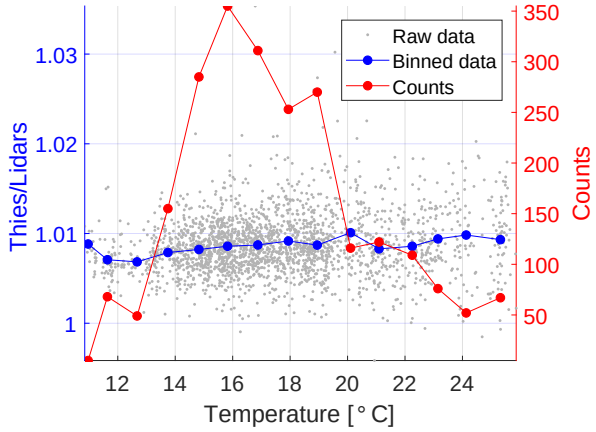

Figure 28. Ratio between horizontal wind speed measured with the Thies cup and the SRWS system as a function of temperature.

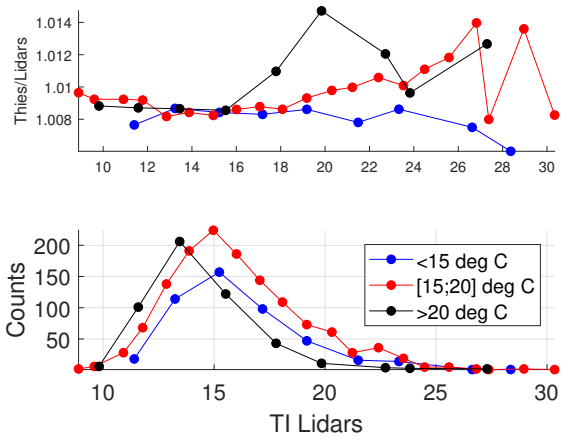

Figure 29. Ratio between horizontal wind speed measured with the Thies cup and the SRWS system as a function of SRWS turbulence intensity. The data is grouped in different temperature intervals.

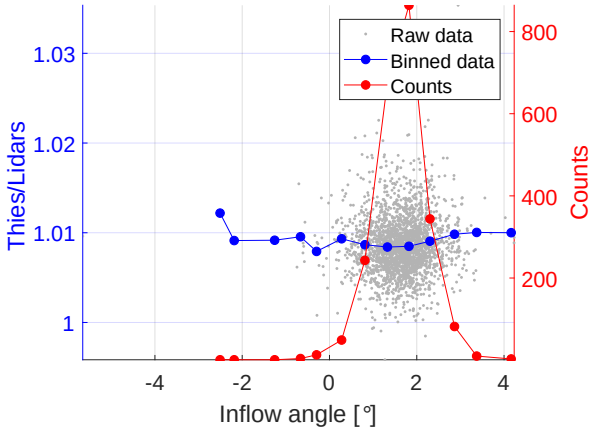

Figure 30. Ratio between horizontal wind speed measured with the Thies cup and the SRWS as a function of inflow angle measured with the SRWS.

6 Discussion

6.1 Comments on the SRWS

The main advantage of the OATR setup is to have the SRWS as reference wind measurement. The SRWS provides the 3D wind vector without disturbing the sensed flow. This is, in theory, an ideal reference for the assessment of the performance of other wind measurement instruments, such as cup anemometer.

However, this experiment has required a lot of unforeseen development and fixing of the SRWS units and data acquisition system: focus adjustment, focus motor jittering, unbalanced detectors on R2D3, R2D2 astigmatism (prism imperfection), data acquisition through DAQWin, choice of Doppler spectra treatment algorithm (treatment of background noise spectra, peak near 0m/s, Doppler frequency estimator). Given the limited time, they may not have been all fixed (e.g. peak near 0m/s) and the accuracy of the SRWS used as reference in this experiment may still be questioned. Nevertheless, those doubts were minimized by:

- Verifying the LOS measurement from each of the WindScanner against a flywheel (this process provides a verification of the right application of the physical constants and algorithms;
- A thorough data quality control of the SRWS data described in this report;
- A general good agreement between the SRWS and the sonic and cup anemometers sequentially mounted on the mast.

The filtering of the SRWS data was rather conservative to ensure the best possible data quality. In particular the despiking algorithm applied to the 20Hz time series was removing a lot of data, including a lot of reliable data, which limited the size of the data set usable for the analysis. In spite of the despiking, the turbulence intensity returned by the SRWS was unexpectedly larger than the cup TI by 4.2%, since the SRWS is measuring over a volume. Further investigation of possible noise in the SRWS signal should be investigated.

Another uncertainty in the SRWS system measurement comes from the setup of the three units at the OATR (positions, beam orientations and beam focus position). Specific care was taken on that part (measurement of the positions with a Leica total station, check of the beam orientations and focus with aligning balls and IR tools, see section 2). Nevertheless, some discrepancies remain unexplained between the SRWS and sonic measurement. Some discrepancy is expected to be due to the sonic probes influence on the flow going through the instrument. However, if that were the only explanation, these results would be similar with all three WindScanner units, whereas the LOS speeds comparison to the projected sonic speed were showing different results for the 3 units (generally good for R2D2, low scatter but average deviation by 4% for R2D1 and large scatter for R2D3). Note that LOS speed error due to peak around 0 in the Doppler spectra was not corrected for (the 10 minute minimum LOS speed was larger than 0.01m/s) for R2D1 in the comparison to the sonic measurements (contrary to the comparison to the cup anemometer).

The measurement height for the OATR was chosen to be 10 m a.g.l. as a compromise to have a mast top mounted cup anemometer, to limit the influence of the ground on the sensed flow and especially for the SRWS to be operated with a small probe volume. Nevertheless, the probe length was between 35 and 48cm for the three units, which actually is still larger than the sonic and cup volume. The SRWS probe length could be reduced by removing the prisms from the optical head. The prism enables the WindScanners to steer the beam in scanning patterns, and are therefore not necessary to measure in staring mode. The probe volume is then expected to be reduced to about 16cm.

Finally, prior to the start of the measurement campaign, we should have identified the best position for the SRWS measurement volume: as close as possible to the cup to get the best correlation and as for as necessary to avoid any influence of the cup anemometer on the SRWS measurement volume. This could have been investigated by scanning the flow along a line at the cup rotor height from 2m before the cup to 2m after.

6.2 Evaluation of the OATR

Could the OATR be used for open air cup calibration? Cup calibrations take place in wind tunnels, which enables consistency and reproducibility of the results thanks to the controlled environment (especially TI level and inflow angle). However those parameters are not representative of the conditions under which the cup anemometer operates once it is installed on a mast in the open air. For example, TI is below 1% in a wind tunnel and expected to be between 5 and 12% in the open air above flat terrain (following flat terrain definition from the IEC 61400-12-1 criteria for terrain complexity) and at about 100m a.g.l. Depending on the response of the cup anemometer (depending on its design) to TI level, this difference could result in a measurement error. The purpose of the cup anemometer classification is to assess this error and provide an uncertainty to account for these possible variations due to environmental parameters including TI, flow inclination, air temperature, air density. Calibrating a cup anemometer in the open air could provide a calibration under "realistic" environmental conditions. However, the calibration would only be valid for the specific conditions ranges of TI, inflow angle, temperature, air density, at this site and in the calibration time period.

The point is not to systematically replace wind tunnel cup anemometer calibration with open air calibration. In particular because it would not be practical as an open air calibration requires at least several days to collect data covering the whole 4 to 16 m/s wind speed range (this could take up to several weeks depending on the wind conditions) whereas it only takes half-an-hour in a wind tunnel. But it could be relevant if one wanted a calibration for the specific range of conditions the anemometer is going to be used in (e.g. for measuring the wind speed during a wind turbine power performance test).

This is an issue with the current location of the OATR. The TI range that occur at this location is much larger than what is expected at a wind turbine hub height (where a large number of cups are expected to be used). If a real interest for calibration of cup anemometer in open air conditions was identified, a more suitable location should be found for the OATR, like for example over flatter terrain and maybe higher up a.g.l., which would require some different set up. Only changing the focus of the SRWS units to a larger height, while the hardware is kept on the ground, would increase the probe volume and would not be suitable anymore. The current design of the SRWS, with large and heavy bodies and complex optics, is therefore not suitable for this purpose. A simpler system, using 3 telescopes with manual focus on fixed stands (which could be mounted in tall masts), for example, would be much more practical.

In this experiment, the cup anemometer wind speed was larger than the WindScanner wind speed. In section 5, we have used the OATR data to try to identify some of the cup anemometer sensitivity to open air conditions. Small sensitivities to wind speed and turbulence intensity were shown. Nevertheless those variations were much smaller than the scatter. Individual 10 min wind speed ratio ranged between 0.999 and 1.034. As those scatter were also observed within each wind direction bin, and the SRWS uncertainty is expected to be small, they are expected to be mainly due to the cup anemometer variations. Nevertheless, the SRWS uncertainty model presented in Appendix D should include some noise in the LOS speed measurement to be more realistic as some noise was detected by the TI measurement comparison (section 4.3).

Could the OATR be used for validation and improvement of the cup classification? An open air classification test would require measurements covering a large range (to extreme values) of all ambient conditions expected to have an influence on the cup anemometer response. That would at best require a very long measurement period (at least one year) and a quite special site where conditions are varying very much (e.g. inflow angle). Alternatively, and probably more realistic, the same cup anemometer could be mounted on several OATRs in different various locations with different atmospheric conditions (e.g. cold climate, high altitude, complex and flat terrains).

The primary purpose of those measurements is actually to validate the Accuwind cup anemometer model used for cup anemometer classification. The SRWS data will be used as input to the model and the simulated 10 min mean wind speeds will be compared to the actual measurements from the cup anemometer. This will enable us to find out how much of the deviation from the tunnel cup calibrations can be explained by the external conditions. This will be the subject of

another report.

7 Conclusions

The report describes the first test of the TrueWind Open Air Test Rig designed to test cup anemometers wind measurements in open air conditions using a Short Range WindScanner system to measure the reference wind speed.

This experiment demonstrated the ability of the SRWS system to provide measurement of the undisturbed flow (contrary to a sonic anemometer for example). In this experiment, the SRWS wind data were streamed directly to the DTU data acquisition system DAQwin for the first time. Thus data from all instruments (especially the test anemometer and the SRWS were recorded simultaneously by the same data acquisition system which enabled an easy and accurate time synchronization of the different systems. This is a first step towards a stable and user friendly set up for this kind of cup testing. In the process of setting up SRWS, we have also identified a number of technical issues. Many of them have been fixed on the way, but further development are required to make the OATR set stable and user-friendly if it should be used for tests with other types of anemometers.

Furthermore, as long as there is no SRWS system (or equivalent) dedicated to the OATR, it is strongly recommended to follow a strict procedure similar to that described in this report regarding:

- the verification of the LOS speed measurement of each SRWS unit, every time a optics or the signal processing software have been modified
- the alignment of the beams and focus ranges, every time a unit has been moved and put back in place.

The current location of the OATR is however not suitable for cup anemometer calibration, if the purpose is to provide a calibration for conditions in which the cup anemometer is to be used (e.g. mounted on a mast at wind turbine hub height); especially because the turbulence intensity is too high due to the terrain relative complexity and the proximity of the ground.

The cup anemometer wind speed was larger than that measured by the SRWS by 0.88%. A sensitivity analysis has been carried out in order to identify if some of the deviation could be explained by the cup anemometer response to the open air wind conditions. Only a small sensitivity to the wind speed and the turbulence intensity could be shown, that were almost insignificant compared to the large scatter in the data. As the SRWS uncertainty mainly includes biases and no random uncertainty, those scatter are expected to be due variations in the cup anemometer response.

Further analysis of these data require simulations using the Accuwind cup model of the cup response to the specific atmospheric conditions. The SRWS data will be used as input to the model. This will be described in another report.

Acknowledgments

We would like to acknowledge Karen Enevoldsen, Steen A. Sørensen, Lars Christensen, Claus Pedersen and Per Hansen from the TEM section of DTU Wind Energy for setting up, running, and maintaining the Truewind experiment. We would also like to thank Torben Mikkelsen, Mikael Sjoholm and Nikolas Angelou (fro the MES section) for their contribution in designing the experiment and preparing the WindScanner system. Finally thanks as well to Alfredo Peña, Jakob Mann and Ebba Delwick for their comments on the data analysis.

A Description of database

The 20 Hz data from the WindScanners has Quality checked (see section 2.4) and has been saved in a database together with the data from the mast. Table 6 give a description of the different columns in the data base.

Column name	Unit	Descriptiotion
Name		Time stamp of the 10-min period. All data in belonging to the same 10-min period will have the same Name
scan_id		Sample id for a sample in each 10-min period. The data is sampled with 20 Hz, so the scan_id goes up to 12000
R2D1_WS	m/s	LOS wind speed measured with WindScanner R2D1. Bad Quality data has been removed as describes in section 2.4.
R2D2_WS	m/s	LOS wind speed measured with WindScanner R2D2. Bad Quality data has been removed as describes in section 2.4.
R2D3_WS	m/s	LOS wind speed measured with WindScanner R2D3. Bad Quality data has been removed as describes in section 2.4.
u	m/s	Reconstructed wind speed in eastern direction. (Positive towards east).
v	m/s	Reconstructed wind speed in western direction.(Positive towards west).
w	m/s	Reconstructed wind speed in vertical direction (Positive up).
correct		Values that indicate whether the data point has been removed. The value is 1 if the data has been removed and 0 if nothing has been done to the data point. The data availability for a 10-min period is given as $1 - \langle \text{correct}_{10min} \rangle$.
T_abs_6m	°C	Temperature measured in 6 m above ground level.
WS_Thies_10m	m/s	Wind speed measured with the Thies cup anemometer mounted in 10 m abouve ground level.
RH_2m	%	Relative humidity measured in 2 m above ground level
Pressure_2m	Pa	Pressure measured 2 m above ground level
Wdir_6m	°	Wind direction measured in 6 m above ground level with a wind vane

Table 6. Description of the different columns in the data base

B Thies cup calibration certificate

DEUTSCHE WINDGUARD

1108/2714

Deutsche WindGuard
Wind Tunnel Services GmbH

IECRE and MEASNET approved test laboratory

accredited by the / *akkreditiert durch die*

Deutsche Akkreditierungsstelle GmbH

as calibration laboratory in the / *als Kalibrierlaboratorium im*

Deutschen Kalibrierdienst

DAkkS Deutsche Akkreditierungsstelle D-K-15140-01-00

Calibration mark *Kalibrierzeichen*	1810801
	D-K-15140-01-00
	02/2018

Calibration certificate
Kalibrierschein

Object *Gegenstand*	Cup Anemometer
Manufacturer *Hersteller*	Thies Clima D-37083 Göttingen
Type *Typ*	4.3351.10.000
Serial number *Fabrikat/Serien-Nr.*	11116755 2714
Customer *Auftraggeber*	DTU Wind Energy DK-4000 Roskilde
Order No. *Auftragsnummer*	Email 2017-12-11, Joergensen
Project No. *Projektnummer*	VT171218
Number of pages *Anzahl der Seiten*	4
Date of Calibration *Datum der Kalibrierung*	20.02.2018

This calibration certificate documents the traceability to national standards, which realize the units of measurement according to the International System of Units (SI).
The DAkkS is signatory to the multilateral agreements of the European co-operation for Accreditation (EA) and of the International Laboratory Accreditation Cooperation (ILAC) for the mutual recognition of calibration certificates.
The user is obliged to have the object recalibrated at appropriate intervals.
Dieser Kalibrierschein dokumentiert die Rückführung auf nationale Normale zur Darstellung der Einheiten in Übereinstimmung mit dem Internationalen Einheitensystem (SI).
Die DAkkS ist Unterzeichner der multilateralen Übereinkommen der European co-operation for Accreditation (EA) und der International Laboratory Accreditation Cooperation (ILAC) zur gegenseitigen Anerkennung der Kalibrierscheine.
Für die Einhaltung einer angemessenen Frist zur Wiederholung der Kalibrierung ist der Benutzer verantwortlich.

Date *Datum*	Head of the calibration laboratory *Leiter des Kalibrierlaboratoriums*	Person in charge *Bearbeiter*
20.02.2018	Dipl. Phys. Dieter Westermann	Techniker Dirk Henninges

1810801
D-K-15140-01-00
02/2018

Calibration object
Kalibriergegenstand

Cup Anemometer

Calibration procedure
Kalibrierverfahren

- Deutsche WindGuard Wind Tunnel Services: VA Anemometerkalibrierung - D5831 Version 13

Based on following standards:

- MEASNET ANEMOMETER CALIBRATION PROCEDURE Version 2 / 2009
- IEC 61400-12-1:2017 Power performance measurements of electricity producing wind turbines
- IEC 61400-12-2:2013 Power performance of electricity producing wind turbines based on nacelle anemometry
- ISO 3966:2008 Measurement of fluid in closed conduits
- ISO 16622:2002 Meteorology - Sonic anemometers/thermometers

Place of calibration
Ort der Kalibrierung

Wind tunnel of Deutsche WindGuard WindTunnel Services GmbH, Varel

Test conditions
Messbedingungen

wind tunnel area	10000 cm²
anemometer frontal area	230 cm²
diameter of mounting pipe	34 mm EN 10217
blockage ratio [1)]	0.023 [-]
software version	7.7

[1)] Due to the special construction of the test section no blockage correction is necessary.

Ambient conditions
Umgebungsbedingungen

air temperature	20.5 °C ± 0.1 °C
air pressure	1020.6 hPa ± 0.3 hPa
relative air humidity	30.0 % ± 2.0 %

Measurement uncertainty
Messunsicherheit

The expanded uncertainty assigned to the measurement results is obtained by multiplying the standard uncertainty by the coverage factor k=2. It has been determined in accordance with DAkkS-DKD-3. The value of the measurand lies within the assigned range of values with a probability of 95%.
The reference flow speed measurement is traceable to the German NMI (Physikalisch-Technische Bundesanstalt) standard for flow speed. It is realized by using a PTB owned and calibrated Laser Doppler Anemometer (Standard Uncertainty 0.2 %, k=2)

Additional remarks
Zusätzliche Anmerkungen

Calibration after refurbishment

1810801
D-K-15140-01-00
02/2018

Calibration result
Kalibrierergebnis

Sensor Hz	Tunnel Speed m/s	Uncertainty m/s
81.650	3.980	0.050
122.756	5.870	0.050
165.851	7.855	0.051
209.188	9.865	0.051
252.857	11.881	0.052
294.724	13.809	0.052
337.876	15.764	0.052
316.758	14.784	0.052
274.748	12.887	0.052
230.880	10.845	0.051
186.665	8.850	0.051
144.876	6.910	0.051
102.049	4.940	0.050

File: 1810801

Statistical analysis

Slope	0.04599 (m/s)/(Hz) ±0.00006 (m/s)/(Hz)
Offset	0.2395 m/s ±0.012 m/s
Standard error (Y)	0.013 m/s
Correlation coefficient	0.99999

Remarks

The calibrated sensor complies with the demanded linearity of MEASNET

Graphical representation of the result
Grafische Darstellung des Ergebnisses

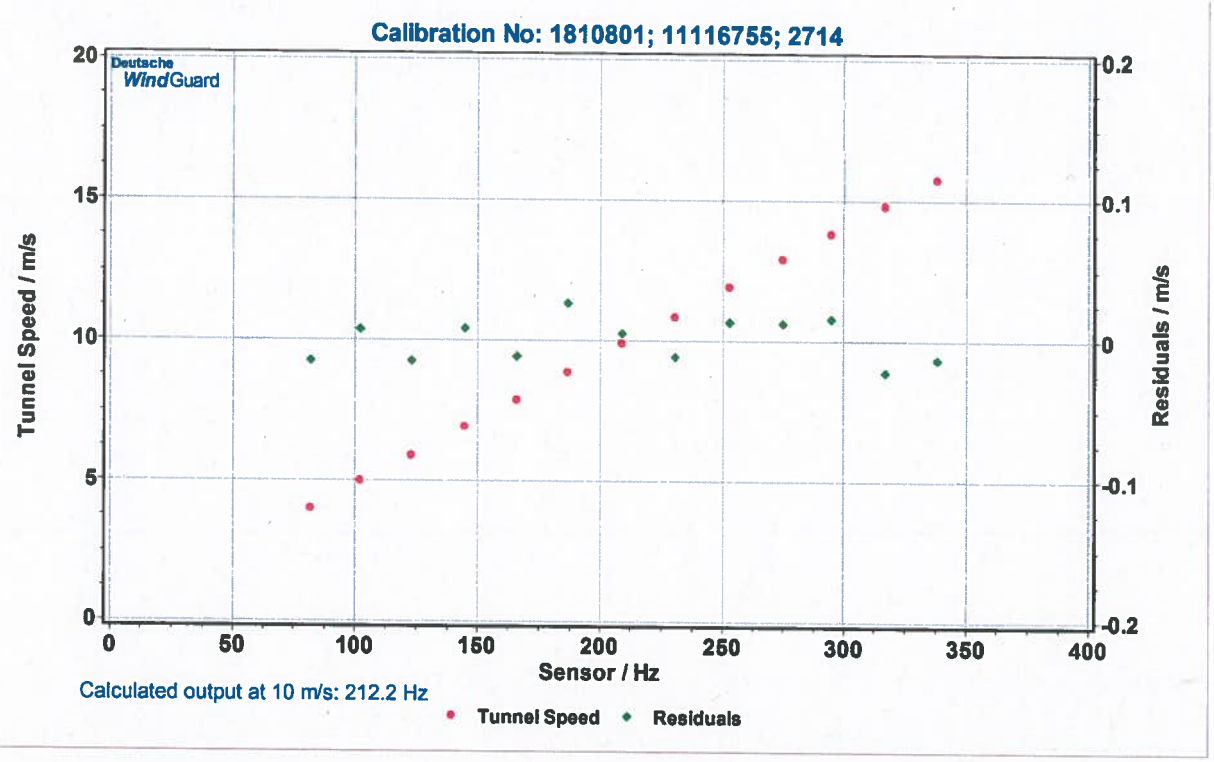

Photo of the measurement setup
Foto des Messaufbaus

Remark: The proportions of the set-up may not be true to scale due to imaging geometry.

C Instrumentation of mast

S4710A TrueWind
Arrangement Drawing Met-Mast

RISØ EQUIPMENT

- RISØ P2426B, P2429, P2029
  Abs. Temp.
- F2919A Vector Windvane W200P
- Metek P2901 USA-1 Sonic 3D
  Support pole P4023A
- F4002D Vaisala PTB110 800...1060 hPa,
  0...5V Air Pressure
- F4025A Thies 1st class
  4.3351.10.000
  Cup Anemometer
- F4607A Rotronic HC2-S3
  Humidity/Temperature probe
  Radiation Shield

MetMast

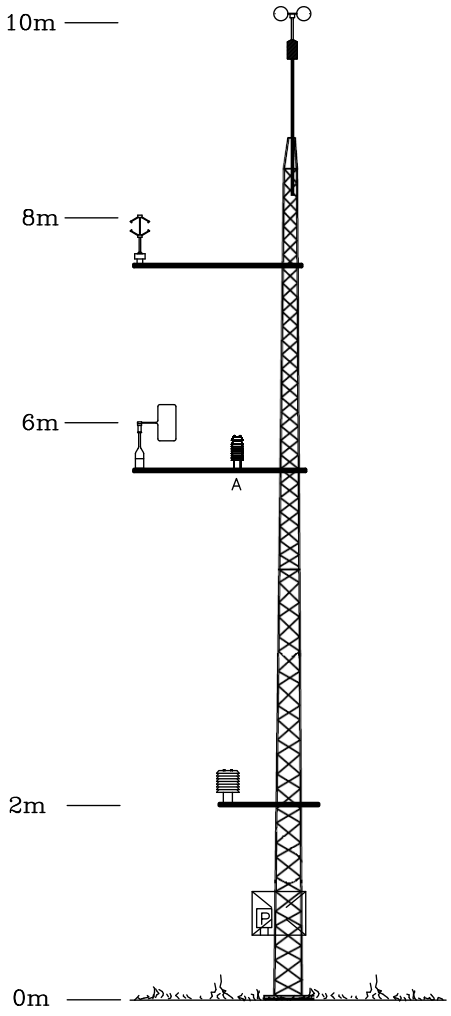

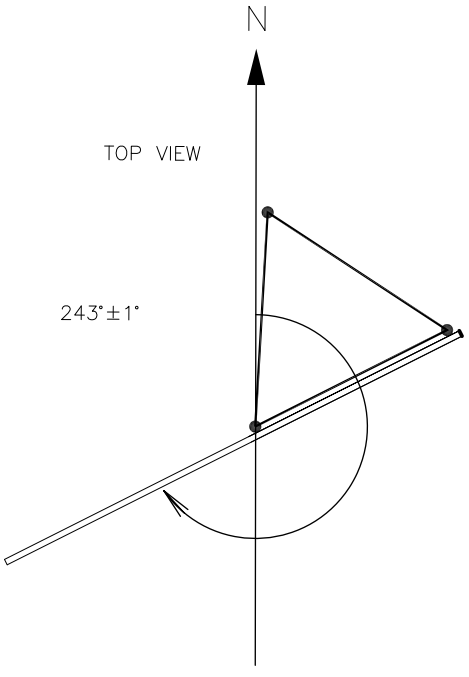

RISØ

DTU Wind Energy

Design by: EJUU 09.05.2017	S4710A, TrueWind.
Re-Drawn by:EJUU 29.03.2019	Risø Metmast
	Top View
SA4710A01-03 Metmast_Interconn..dwg	sheet 1 of 1

S4710A TrueWind
Arrangement Drawing Met-Mast

RISØ EQUIPMENT

- RISØ P2426B, P2429, P2029
  Abs. Temp.
- F2919A Vector Windvane W200P
- Metek P2901 USA-1 Sonic 3D
  Support pole P4023A
- F4002D Vaisala PTB110 800...1060 hPa,
  0...5V Air Pressure
- F4025A Thies 1st class
  4.3351.10.000
  Cup Anemometer
- F4607A Rotronic HC2-S3
  Humidity/Temperature probe
  Radiation Shield

MetMast

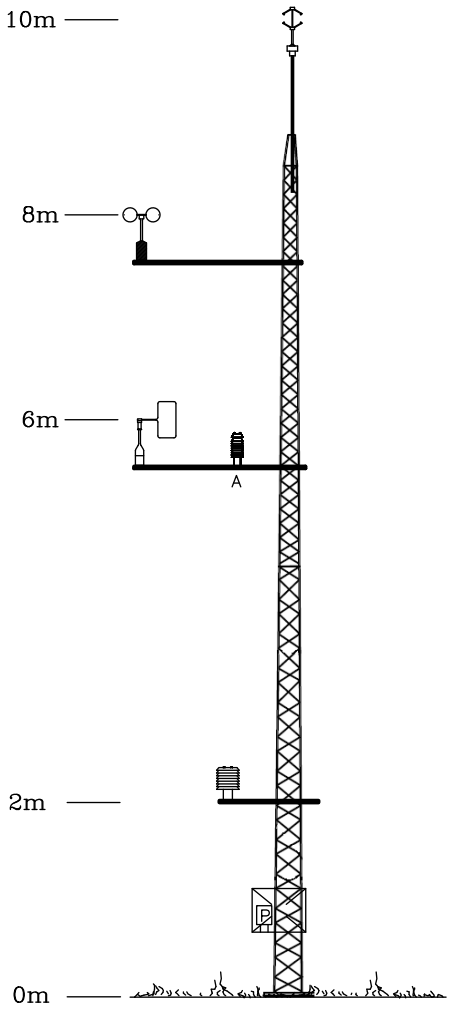

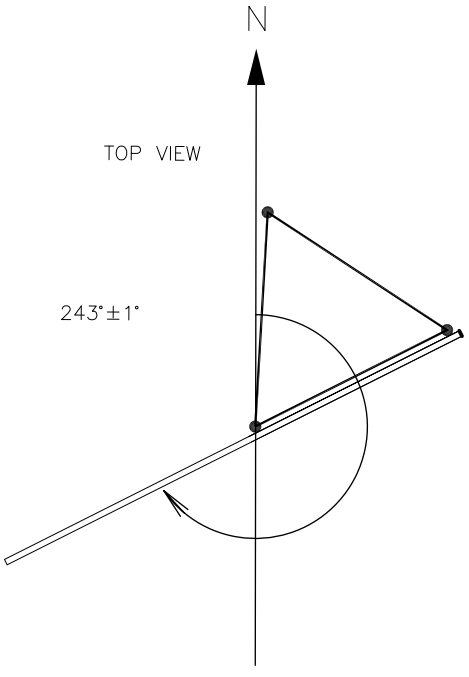

RISØ

DTU Wind Energy

Design by: EJUU 09.05.2017	S4710A, TrueWind.
Re-Drawn by:EJUU 29.03.2019	Risø Metmast
	Top View
SA4710A01-04 Metmast_Interconn..dwg	sheet 1 of 1

D Velocity reconstruction and uncertainty estimation

As is well known, a wind lidar measures only the component of the wind velocity along the laser beam (line of sight). If the wind velocity is given by the vector (u,v,w) the line of sight speed (or radial speed) measured by a lidar is

$$V_r = u\sin\theta\cos\phi + v\cos\theta\cos\phi + w\sin\phi, \tag{D.10}$$

where θ is the azimuth and ϕ the elevation angle (measured from horizontal) of the beam direction, and defined in Fig. 31.

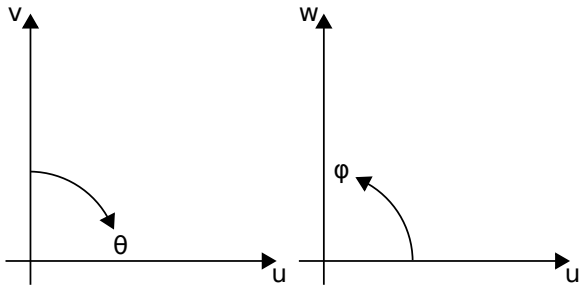

Figure 31. Definition of the azimuth, θ, and elevation, ϕ, angles of the beam direction in the coordinate system of the wind vector (u,v,w). This could typically, but not necessarily, be defined such that u points towards East and v towards North meaning that θ follows the normal compass bearing definition.

D.1 Reconstructing *u*, *v*, and *w*

In order to derive the three dimensional wind velocity it is necessary to have three simultaneous measurements of V_r from three lidars resulting in three equations of the same kind as Eq. (D.10). These equations can be solved for u, v, and w with the following result

$$\begin{aligned} u = &[V_1(\alpha_2\sin\phi_3 - \alpha_3\sin\phi_2) + \\ &V_2(\alpha_3\sin\phi_1 - \alpha_1\sin\phi_3) + \\ &V_3(\alpha_1\sin\phi_2 - \alpha_2\sin\phi_1)] / (a\sin\phi_1 + b\sin\phi_2 + c\sin\phi_3), \end{aligned} \tag{D.11}$$

$$\begin{aligned} v = &[V_1(\beta_3\sin\phi_2 - \beta_2\sin\phi_3) + \\ &V_2(\beta_1\sin\phi_3 - \beta_3\sin\phi_1) + \\ &V_3(\beta_2\sin\phi_1 - \beta_1\sin\phi_2)] / (a\sin\phi_1 + b\sin\phi_2 + c\sin\phi_3), \end{aligned} \tag{D.12}$$

$$w = [aV_1 + bV_2 + cV_3] / (a\sin\phi_1 + b\sin\phi_2 + c\sin\phi_3), \tag{D.13}$$

where

$$\alpha_i = \cos\theta_i \cos\phi_i,$$
$$\beta_i = \sin\theta_i \cos\phi_i,$$
$$a = \alpha_3\beta_2 - \alpha_2\beta_3,$$
$$b = \alpha_1\beta_3 - \alpha_3\beta_1,$$
$$c = \alpha_2\beta_1 - \alpha_1\beta_2.$$

The denominator in Eq. (D.11-D.13) can more explicitly be written

$$\begin{aligned} a\sin\phi_1 + b\sin\phi_2 + c\sin\phi_3 = &\sin(\theta_2-\theta_3)\sin\phi_1\cos\phi_2\cos\phi_3 \\ &+\sin(\theta_3-\theta_1)\cos\phi_1\sin\phi_2\cos\phi_3 \\ &+\sin(\theta_1-\theta_2)\cos\phi_1\cos\phi_2\sin\phi_3. \end{aligned}$$

From u and v the horizontal wind speed, V_h, and direction, Θ, can be calculated

$$V_\mathrm{h} = \sqrt{u^2+v^2}, \tag{D.14}$$

$$\Theta = \arctan\left(\frac{-u}{-v}\right), \tag{D.15}$$

with Θ defined as the meteorological wind direction.

D.2 Estimation of uncertainties

Measurement uncertainties can be estimated in a number of ways, but here will be briefly described two of the most frequently used methods; the so-called GUM approach, [7], and Monte Carlo simulations.

The GUM approach gives the mathematical framework for calculating the uncertainty based on a so-called model equation, $M(x_1,\ldots)$. Following this approach the combined standard uncertainty, U, of an estimate is found as

$$U = k\cdot\sqrt{\sum_{i=1}^{k} u_{x_i}^2 c_{x_i}^2}, \tag{D.16}$$

where k is the coverage factor, u_{x_i} are the uncertainties associated with each of the input estimates, and the influence coefficients, $c_{x_i} = \frac{\partial}{\partial x_i}$, are the partial derivatives of the model equation with respect to the same input.

If the uncertainty of the input variables are correlated, which is indeed very often the case, Eq. (D.16) needs to be expanded and becomes

$$U = k\cdot\sqrt{\sum_{i=1}^{k} u_{x_i}^2 c_{x_i}^2 + 2\sum_{i=1}^{k-1}\sum_{j=i+1}^{k} c_{x_i}c_{x_j}u_{x_i}u_{x_j}r_{x_ix_j}}, \tag{D.17}$$

where $r_{x_ix_j}$ is correlation coefficient between two correlated input variables.

Another way of estimating uncertainties is to use Monte Carlo simulations. In short, this method is about letting a computer calculate many (thousands or millions) outputs of the model equation where each time the inputs are chosen randomly from a distribution based on their uncertainty. The distribution of the outputs are then used as a measure of the uncertainty.

In this document we will use the GUM approach, under the assumption that the uncertainties of the input variables are uncorrelated, to estimate the uncertainties of horizontal wind speed and direction obtained from the OATR setup.

D.2.1 Uncertainty of beam azimuth and elevation angles

The beam azimuth and elevation angles are calculated from measurements of the positions of the beam outputs from scan heads and positions on the alignment ball made with the Leica Total-Station and given as Eastings, Northings, and Height, $\{e,n,h\}$ in metres. The azimuth angle is thus

$$\theta = \arctan\left(\frac{e}{n}\right) = \arctan\left(\frac{e_s - e_b}{n_s - n_b}\right), \tag{D.18}$$

where the subscripts s and b refers to 'scanner' and 'ball', respectively. In order to estimate the uncertainty we apply the GUM approach and assume for convenience that the uncertainties are uncorrelated. The influence coefficients are the partial derivatives of the model equation, Eq. D.18,

$$\frac{\partial\theta}{\partial e_s} = -\frac{\partial\theta}{\partial e_b} = \frac{(n_s - n_b)}{(n_s - n_b)^2 + (e_s - e_b)^2}, \tag{D.19}$$

$$\frac{\partial\theta}{\partial n_s} = -\frac{\partial\theta}{\partial_b} = \frac{-(n_s - n_b)}{(n_s - n_b)^2 + (e_s - e_b)^2}. \tag{D.20}$$

and the combined uncertainty becomes

$$U_\theta = \sqrt{\left(u_{e_s}\frac{\partial\theta}{\partial e_s}\right)^2 + \left(u_{e_b}\frac{\partial\theta}{\partial e_b}\right)^2 + \left(u_{n_s}\frac{\partial\theta}{\partial n_s}\right)^2 + \left(u_{n_b}\frac{\partial\theta}{\partial n_b}\right)^2}. \tag{D.21}$$

In a similar way the influence coefficients and combined uncertainty relating to the elevation angle can be calculated from the following model equation

$$\begin{aligned}
\phi &= \arcsin\left(\frac{h}{\sqrt{e^2+n^2+h^2}}\right) \\
&= \arcsin\left(\frac{h_s - h_b}{\sqrt{(e_s-e_b)^2+(n_s-n_b)^2+(h_s-h_b)^2}}\right) \\
&= \arcsin\left(\frac{h_s - h_b}{D_{sb}}\right),
\end{aligned} \tag{D.22}$$

where D_{sb} is the distance from the scanner to the alignment ball. The influence coefficients then become

$$\frac{\partial\phi}{\partial e_s} = -\frac{\partial\phi}{\partial e_b} = \frac{-(e_s - e_b)(h_s - h_b)}{D_{sb}^2\sqrt{(e_s-e_b)^2+(n_s-n_b)^2}}, \tag{D.23}$$

$$\frac{\partial\phi}{\partial n_s} = -\frac{\partial\phi}{\partial n_b} = \frac{-(n_s - n_b)(h_s - h_b)}{D_{sb}^2\sqrt{(e_s-e_b)^2+(n_s-n_b)^2}}, \tag{D.24}$$

$$\frac{\partial\phi}{\partial h_s} = \frac{\partial\phi}{\partial h_b} = \frac{\sqrt{(e_s-e_b)^2+(n_s-n_b)^2}}{D_{sb}^2}, \tag{D.25}$$

and finally the combined uncertainty

$$\begin{aligned}
U_\phi^2 = &\left(u_{e_s}\tfrac{\partial\phi}{\partial e_s}\right)^2 + \left(u_{e_b}\tfrac{\partial\phi}{\partial e_b}\right)^2 + \left(u_{n_s}\tfrac{\partial\phi}{\partial n_s}\right)^2 + \\
&\left(u_{n_b}\tfrac{\partial\phi}{\partial n_b}\right)^2 + \left(u_{h_s}\tfrac{\partial\phi}{\partial h_s}\right)^2 + \left(u_{h_b}\tfrac{\partial\phi}{\partial h_b}\right)^2.
\end{aligned} \tag{D.26}$$

From the setup and alignment of the instruments we make the following estimates of the beam position measurements

$$\begin{aligned}
u_{e_s} = u_{n_s} = u_{h_s} = 1 \text{ cm}, \\
u_{e_b} = u_{n_b} = u_{h_b} = 5 \text{ cm},
\end{aligned} \tag{D.27}$$

from which we can calculate the uncertainties given in Table 7 by using Eqs. (D.21) and (D.26). In this table is also stated an uncertainty of 0.2% for the radial velocity estimation and that is based on the results from a lidar calibration using a rotating wheel, [12].

	U_θ	U_ϕ	V_r
R2D1	0.31°	0.23°	0.2%
R2D2	0.34°	0.24°	0.2%
R2D3	0.40°	0.26°	0.2%

Table 7. Estimated uncertainties of beam azimuth and elevation angles together with the radial velocity estimation uncertainty.

D.2.2 Uncertainty of u, v, and w due to pointing and V_r estimation uncertainties

Now that the azimuth and elevation angle uncertainties have been found they can be used to derive the uncertainties for u, v, and w; again following the GUM approach. In this case the model equations are Eqs. (D.11), (D.12), and (D.13) and in order to find the influence coefficients it is beneficial to write these in a general form as the ratio between two functions F and G

$$\begin{aligned} M_{u,v,w}(\theta_1,\theta_2,\theta_3,\phi_1,\phi_2,\phi_3) &= \frac{F(\theta_1,\theta_2,\theta_3,\phi_1,\phi_2,\phi_3)}{G(\theta_1,\theta_2,\theta_3,\phi_1,\phi_2,\phi_3)} \\ &= \frac{f_{V_1}+f_{V_2}+f_{V_3}}{G}, \end{aligned} \tag{D.28}$$

where the subscripts V_{1-3} denotes from which term in the model equation it originates. A general expression for the partial derivatives can then be found as

$$\begin{aligned} \frac{\partial M_{u,v,w}}{\partial x} = \frac{\frac{\partial F}{\partial x}\cdot G - F\cdot\frac{\partial G}{\partial x}}{G^2} &= \frac{\left(\frac{\partial f_{V_1}}{\partial x}+\frac{\partial f_{V_2}}{\partial x}+\frac{\partial f_{V_3}}{\partial x}\right)\cdot G - F\cdot\frac{\partial G}{\partial x}}{G^2} \\ &= \frac{\frac{\partial f_1}{\partial x}+\frac{\partial f_2}{\partial x}+\frac{\partial f_3}{\partial x} - M\cdot\frac{\partial G}{\partial x}}{G}, \end{aligned} \tag{D.29}$$

which can then be inserted in Eq. (D.16) to give the combined uncertainty.

D.2.3 Uncertainty of wind speed, V_h, and direction, Θ

Once the uncertainties of u and v have been found the same method can be applied to calculate the uncertainties of V_h and Θ

$$U_{V_\mathrm{h}} = \sqrt{\left(U_u\frac{\partial V_h}{\partial u}\right)^2+\left(U_v\frac{\partial V_h}{\partial v}\right)^2} = \sqrt{\left(U_u\frac{u}{V_h}\right)^2+\left(U_v\frac{v}{V_h}\right)^2}, \tag{D.30}$$

and

$$U_\Theta = \sqrt{\left(U_u\frac{\partial \Theta}{\partial u}\right)^2+\left(U_v\frac{\partial \Theta}{\partial v}\right)^2} = \sqrt{\left(U_u\frac{v}{V_h^2}\right)^2+\left(U_v\frac{-u}{V_h^2}\right)^2}. \tag{D.31}$$

D.2.4 Results

Numerical estimates of the uncertainties of V_h and Θ can finally be made by inserting the appropriate influence coefficients given by Eqs. (D.29,D.30,D.31) into Eq. (D.16). In this section will be shown some representative examples of U_{V_h} and U_Θ as function of wind speed as well as direction from which a general level of uncertainties can be inferred.

Figure 32 shows the estimated GUM approach uncertainties ($k = 1$) of horizontal wind speed and direction as function of wind direction for an input of 8 m/s horizontal wind speed. The relative wind speed uncertainty oscillates around an average value of about 0.475% with minimum and maximum values of around 0.45% and 0.495%, respectively. A slight asymmetry is observed in the peak values and this is due to the internal azimuth angles between the scanners are not perfectly 120°. The same general behaviour is seen for the uncertainty on wind direction. Here the average value is around 0.292° with minima and maxima of about 0.28° and 0.303°, respectively.

Figure 33 shows the absolute and relative uncertainty on horizontal wind speed as function of wind speed. The uncertainty have been calculated for ten different wind directions equally spaced

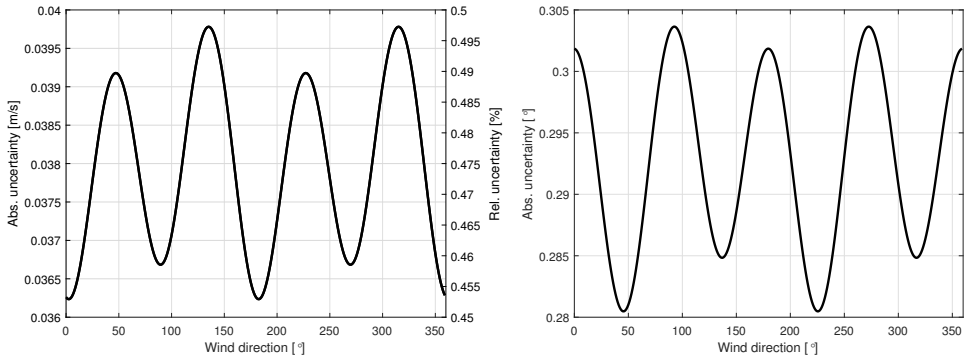

Figure 32. Estimated uncertainties as function of wind direction with an input horizontal wind speed of 8 m/s. Left pane shows the absolute and relative uncertainties on the horizontal wind speed and the right pane shows the absolute uncertainty on the estimated wind direction.

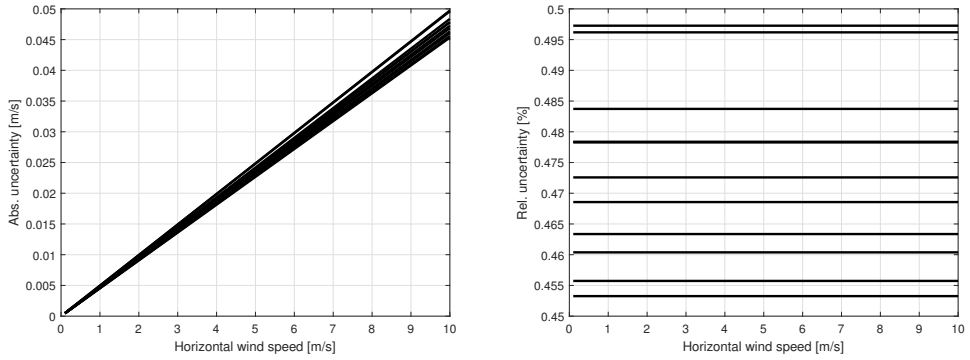

Figure 33. Horizontal wind speed uncertainty as function of wind speed for various input directions.

over the full circle by 35° to cover the differences seen in Figure 32. The uncertainty depends linearly on the input wind speed which can be clearly seen in both plots. The right-side pane shows that the relative uncertainty as expected is independent of input wind speed, but that the input direction leads to a band of uncertainties covering from about 0.45% to 0.5%.

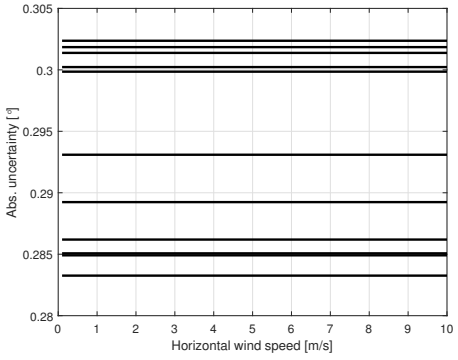

Figure 34. Wind direction uncertainty as function of wind speed for various input directions.

Figure 34 shows the absolute uncertainty of wind direction as function of wind speed for the same ten input directions as used above. Again we see the input directions leading to a spread in the uncertainty ranging from around 0.285° to 0.302°.

References

[1] Leica total stations. `https://leica-geosystems.com/products/total-stations`. Accessed: 2019-03-28.

[2] Metek usa-1. `https://metek.de/product/usonic-3-scientific/`. Accessed: 2019-04-03.

[3] Cyrus F Abari, Anders T Pedersen, and Jakob Mann. An all-fiber image-reject homodyne coherent doppler wind lidar. *Optics express*, 22(21):25880–25894, 2014.

[4] Nikolas Angelou, Farzad Foroughi Abari, Jakob Mann, Torben Mikkelsen, and Mikael Sjöholm. Challenges in noise removal from doppler spectra acquired by a continuous-wave lidar. In *26th International Laser Radar Conference*, 2012.

[5] J.-Å. Dahlberg, Troels Friis Pedersen, and P. Busche. *ACCUWIND - Methods for classification of cup anemometers*. 2006.

[6] JÅ Dahlberg, TF Pedersen, and D Westermann. Development of a standardised cup anemometer suited to wind energy applications, classcup. In *2001 European Wind Energy Conference and Exhibition (EWEC'01)*. WIP Renewable Energies, 2001.

[7] Joint Committee for Guides in Metrology. Jcgm 100: Evaluation of measurement data - guide to the expression of uncertainty in measurement. Technical report, JCGM, 2008.

[8] Derek G Goring and Vladimir I Nikora. Despiking acoustic doppler velocimeter data. *Journal of hydraulic engineering*, 128(1):117–126, 2002.

[9] Ulf Högström and Ann-Sofi Smedman. Accuracy of sonic anemometers: laminar wind-tunnel calibrations compared to atmospheric in situ calibrations against a reference instrument. *Boundary-layer meteorology*, 111(1):33–54, 2004.

[10] IEC. IEC 61400-12-1. Wind turbines – Part 12-1: Power performance measurements of electricity producing wind turbines. International standard, International Electrotechnical Commission, Geneva, Switzerland, 2017.

[11] KH Papadopoulos, NC Stefantos, U Schmidt Paulsen, and E Morfiadakis. Effects of turbulence and flow inclination on the performance of cup anemometers in the field. *Boundary-Layer Meteorology*, 101(1):77–107, 2001.

[12] Anders Tegtmeier Pedersen and Mike Courtney. Flywheel calibration of a continuous wave, coherent doppler wind lidar. to be submitted to Atmospheric Measurement Techniques, June 2019.

[13] Troels Friis Pedersen, J-Å Dahlberg, and Peter Busche. Accuwind-classification of five cup anemometers according to iec 61400-12-1. 2006.

[14] Troels Friis Pedersen and Uwe Schmidt Paulsen. A procedure for classification of cup-anemometers. In *1997 European Wind Energy Conference*, 1997.

[15] Alfredo Peña, Ebba Dellwik, and Jakob Mann. A method to assess the accuracy of sonic anemometer measurements. *Atmospheric Measurement Techniques*, 12(1):237–252, 2019.

[16] Alfredo Peña, Jakob Mann, and Nikolay Krasimirov Dimitrov. Turbulence characterization from a forward-looking nacelle lidar. *Wind Energy Science*, 2(1):133–152, 2017.

[17] Mikael Sjöholm, Nikolas Angelou, Per Hansen, Kasper Hjorth Hansen, Torben Mikkelsen, Steinar Haga, Jon Arne Silgjerd, and Neil Starsmore. Two-dimensional rotorcraft downwash flow field measurements by lidar-based wind scanners with agile beam steering. *Journal of Atmospheric and Oceanic Technology*, 31(4):930–937, 2014.